The Journal of Physiology

Sympathetic stimulation can compensate for hypocalcaemia-induced bradycardia in human and rabbit sinoatrial node cells

Moritz Linder[1], Tomas Stary[1], Gergő Bitay[2], Norbert Nagy[2] and Axel Loewe[1]

[1] *Institute of Biomedical Engineering, Karlsruhe Institute of Technology (KIT), Karlsruhe, Germany*
[2] *Department of Pharmacology and Pharmacotherapy, Albert Szent-Györgyi Medical School, University of Szeged, Szeged, Hungary*

Handling Editors: Bjorn Knollmann & Viviane Timmermann

The peer review history is available in the Supporting Information section of this article (https://doi.org/10.1113/JP287557#support-information-section).

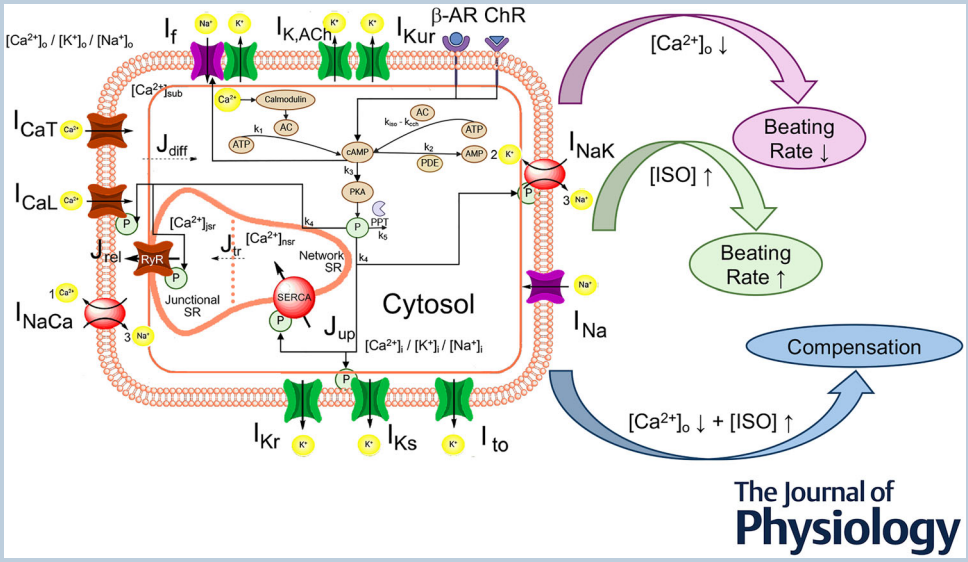

Abstract figure legend AC: adenylyl cyclase, APT: adenosine triphosphate, AMP: adenosine monophosphate, cAMP: cyclic adenosine monophosphate, PDE: phosphodiesterase, PKA: protein kinase A, PPT: protein phosphatase, P: phosphorylation, RyR: ryanodine receptor, SERCA: sarcoplasmic/endoplasmic reticulum Ca^{2+}-adenosine triphosphatase, SR: sarcoplasmic reticulum, β-AR: β-adrenergic receptor, $[Ca^{2+}]_{i/o}$: intra-/extracellular calcium concentration, $[Ca^{2+}]_{jsr/nsr}$: junctional/network sarcoplasmic reticulum calcium concentration, $[Ca^{2+}]$sub: sub-sarcolemmal calcium concentration, ChR: cholinergic receptor, $[K^+]_{i/o}$: intra-/extracellular potassium concentration, $[Na^+]_{i/o}$: intra-/extracellular sodium concentration, [ISO]: isoprenaline concentration, I_{CaL}: L-type Ca^{2+} current, I_{CaT}: T-type Ca^{2+} current, I_f: hyperpolarisation-activated 'funny' current, $I_{K,ACh}$: acetylcholine-activated K^+ current, I_{Kr}: rapidly activating delayed rectifier current, I_{Ks}: slowly activating delayed rectifier current, I_{Kur}: ultra-rapid activating delayed rectifier current, I_{NaCa}: Na^+/Ca^{2+} exchanger current, I_{NaK}: Na^+/K^+ pump current, I_{Na}: Na^+ current, I_{to}: transient outward K^+ current, J_{diff}: Ca^{2+} diffusion flux from submembrane space to myoplasm, J_{rel}: Ca^{2+} release flux from SR via RyRs, J_{tr}: Ca^{2+} diffusion flux from the network to junctional SR, J_{up}: Ca^{2+} uptake by SR.

Moritz Linder is a PhD candidate and research assistant at the Institute of Biomedical Engineering (IBT) of Karlsruhe Institute of Technology (KIT). His research focuses on computational modelling and simulation of the sinoatrial node under various health conditions. Supervised by Dr Axel Loewe his work aims to elucidate the underlying pathomechanisms that contribute to the increased incidence of sudden cardiac death in patients suffering from chronic kidney disease.

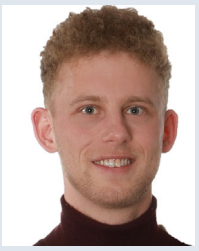

DOI: 10.1113/JP287557

Abstract Regular activation of the heart originates from cyclic spontaneous depolarisations of sinoatrial node cells (SANCs). Variations in electrolyte levels, commonly observed in haemodialysis (HD) patients, and the autonomic nervous system (ANS) profoundly affect the SANC function. Thus we investigated the effects of hypocalcaemia and sympathetic stimulation on the SANC beating rate (BR). The β-adrenergic receptor (β-AR) signalling cascade, as described by Behar et al., was incorporated into the SANC models of Severi et al. (rabbit) and Fabbri et al. (human). Simulations were conducted across various extracellular calcium ($[Ca^{2+}]_o$) (0.6–1.8 mM) and isoprenaline concentrations [ISO] (0–1000 nM) for a sufficient period of time to allow transient oscillations to equilibrate and reach a limit cycle. The β-AR cell response of the extended models was validated against new Langendorff-perfused rabbit heart experiments and literature data. The extended models revealed that decreased $[Ca^{2+}]_o$ necessitated an exponential-like increase in [ISO] to restore the basal BR. Specifically at 1.2 mM $[Ca^{2+}]_o$, the Severi and Fabbri models required 28.0 and 9.6 nM [ISO], respectively, to restore the initial BR. Further reduction in $[Ca^{2+}]_o$ to 0.6 mM required 170.0 and 43.6 nM [ISO] to compensate for hypocalcaemia. A sudden loss of sympathetic tone at low $[Ca^{2+}]_o$ resulted in a loss of automaticity within seconds. These findings suggest that hypocalcaemic bradycardia can be compensated for by an elevated sympathetic tone. The integration of the β-AR pathways led to a logarithmic BR increase and offers insights into potential pathomechanisms underlying sudden cardiac death (SCD) in HD patients.

(Received 28 August 2024; accepted after revision 31 January 2025; first published online 27 February 2025)
Corresponding author M. Linder, Institute of Biomedical Engineering, Karlsruhe Institute of Technology (KIT), Karlsruhe, Germany. Email: moritz.linder@kit.edu

Key points

- We extended the sinoatrial node cell (SANC) models of Severi et al. (rabbit) and Fabbri et al. (human) using the β-adrenergic receptor (β-AR) signalling cascade Behar et al. described.
- Simulations were conducted across various extracellular calcium ($[Ca^{2+}]_o$) (0.6–1.8 mM) and isoprenaline concentrations [ISO] (0–1000 nM) to reflect conditions in haemodialysis (HD) patients.
- An exponential-like increase in [ISO] compensated for hypocalcaemia-induced bradycardia in both models, whereas interspecies differences increased the sensitivity of the extended Fabbri model towards hypocalcaemia and increased sympathetic tone.
- The extended models may help to further understand the pathomechanisms of several cardiovascular diseases affecting pacemaking, such as the high occurrence of sudden cardiac death (SCD) in chronic kidney disease (CKD) patients.

Introduction

The natural cardiac pacemaking function is initiated by periodic excitations of sinoatrial node cells (SANCs), orchestrated by the intricate interplay of the calcium (Ca^{2+}) and membrane currents, known as the coupled clock mechanism. This involves precise regulation of the sensitive balance of inward and outward transmembrane currents during the diastolic depolarisation (DD) phase, as well as the complex interaction of both effects throughout the action potential (AP). Various factors, including the extracellular milieu and the autonomic nervous system (ANS), regulate sinus node electrophysiology, thereby influencing the beating rate (BR) (Kohajda et al., 2020). By precisely regulating electrolyte concentrations in the blood and extracellular milieu, the kidneys are vital for maintaining homeostasis. However in individuals suffering from chronic kidney disease (CKD), the renal system fails to keep the electrolyte levels within these narrow ranges [extracellular calcium concentration ($[Ca^{2+}]_o$) rabbits: 1.60–1.82 mmol/l (Harcourt-Brown, 2002), humans: 1.16–1.32 mmol/l (Bell, 1995)], contributing to a 14-fold increase in the risk of sudden cardiac death (SCD) compared to patients with cardiovascular disease and normal kidney function (Di Lullo et al., 2016). Long-term studies in haemodialysis (HD) patients with implantable loop recorders revealed that all observed SCDs occurred after progressive bradycardia followed by asystole rather than the traditional SCD mechanisms such as ventricular

tachycardia or ventricular fibrillation (Sacher et al., 2018). Thus attention turned to bradycardia and asystole as important pathomechanisms, which might be explained by the fluctuations in electrolyte concentrations caused by HD or renal failure.

Loewe, Lutz, Nairn et al. (2019) investigated the effect of altered electrolyte levels on sinus node pacemaking, highlighting that hypocalcaemia, in particular, slows down the BR. Furthermore the ANS is frequently dysfunctional and imbalanced in HD patients with sympathetic overactivity driven by afferent sensory renal nerves stimulated by renal injury (Poulikakos et al., 2014). CKD was also associated with a reduced BR response to sympathetic stimulation, and it was found that an abrupt reduction in sympathetic tone acutely precedes SCD in a rat model (Zhao et al., 2016). Moreover Santini et al. (2024) reported a unique case of an 80-year-old woman who experienced sinus arrest followed by bradycardia, which was caused by severe iatrogenic hypocalcaemia. Normal sinus node function was successfully restored during the hospitalisation by correcting the electrolyte levels with calcitriol.

In this study we tested the hypothesis that an increased sympathetic tone can compensate for hypocalcaemia-induced bradycardia to a certain extent, whereas a sudden loss under hypocalcaemic conditions could lead to severe bradycardia and SCD in CKD patients. We studied this in computational models of rabbit and human SANCs. Current computational models barely allow for simulation of graded ANS effects, such as β-adrenergic receptor (β-AR) stimulation of membrane and sarcoplasmic reticulum (SR) currents. There is an attempt at linear interpolation of conductance increases and gate shifts by Stary et al. (2023) and a phenomenological approach by Maltsev and Lakatta (2010). Demir et al. (1999) proposed a cascade in which only cAMP modulated target ion channels, and Himeno et al. (2008) developed a guinea-pig SANC model without consideration of subsarcolemmal space, resulting in low intracellular Ca^{2+} levels during local Ca^{2+} release. Thus, we extended the SANC models of Severi et al. (2012) (rabbit) and Fabbri et al. (2017) (human) using the β-AR signalling cascade, which also takes the adenylyl cyclase (AC)-cAMP-protein kinase A (PKA) interplay into account, as suggested by Behar et al. (2016). The β-AR cell response of the extended model was validated by experiments using Langendorff-perfused rabbit hearts under the influence of various isoprenaline [ISO] and $[Ca^{2+}]_o$. This allowed us to investigate the compensatory effect of [ISO] on hypocalcaemia-induced bradycardia and interspecies differences in mammalian pacemaking (Loewe, Lutz, Nagy et al., 2019).

Methods

Langendorff-perfused heart experiments

Ten female and male New Zealand white rabbits weighing 2–2.5 kg were used for the Langendorff-perfused heart experiments. The animals were housed in a conventional animal house, in cages, which conformed to the size recommendations in the most recent Guide for the Care and Use of Laboratory Animals DHEW (NIH) and EU Guidelines 63/2010. The litter material placed beneath the cage was changed at least twice a week. The animal room was humidity monitored and temperature controlled, had a 12 h light–dark cycle with lights switched on from 7:00 AM to 7:00 PM and was kept clean and vermin free. The animals were acclimatised in the housing facilities for at least 3 days prior to testing. Standard rabbit chow and filtered tap water were provided *ad libitum*. There were no known contaminants reasonably expected to be found in the food or water at levels, which would have interfered with the results of this study based on periodic reports provided by Szeged municipal waterworks.

Rabbits were anticoagulated with sodium heparin (1000 IU) and anaesthetised with sodium pentobarbital (∼80 mg/kg), both administered through the marginal ear vein. Non-invasive blood pressure (NIBP) and heart rate were measured using an InnoCare-VET (Innomed Medical Ltd, Budapest, Hungary) patient monitor. The depth of anaesthesia was monitored by observing autonomic parameters. Anaesthesia was considered sufficient when the heart rate stabilised and did not increase in response to a surgical incision. Similarly adequate depth was confirmed if blood pressure remained stable despite a standard surgical incision. Additionally the absence of pupil dilatation was interpreted as a lack of sympathetic response, indicating satisfactory anaesthesia depth. Then hearts were immediately removed via thoracotomy and rinsed in ice-cold modified Krebs–Henseleit buffer, containing (in mM): $NaHCO_3$, 25; KCl, 4.3; NaCl, 118.5; $MgSO_4$, 1.2; KH_2PO_4, 1.2; glucose, 10; $CaCl_2$, 1.8, with pH 7.4 ± 0.05 when gassed with 95% O_2 and 5% CO_2.

The excised hearts were mounted by the aorta on a Langendorff apparatus and retrograde perfused with modified Krebs–Henseleit solution at constant pressure (80 mmHg). The electrical activity measured as an ECG) was obtained using three lead custom-made electrodes and signal amplifier (Experimetria Ltd, Budapest, Hungary). Signal processing and analysis was carried out using HaemoSys (Experimetria Ltd). After control recordings, various concentrations of isoprenaline (ISO, Merck Life Science Ltd, Darmstadt, Germany) were employed, and the ECG R–R intervals were analysed. All experiments were carried out at 37°C.

Model adjustments

We analysed the concentration-dependent compensatory effect of various [ISO] in reference to decreasing $[Ca^{2+}]_o$ in the *in silico* SANC models of Severi et al. (2012) (rabbit) and Fabbri et al. (2017) (human). Therefore the model definitions were acquired from the CellML (Cuellar et al., 2003) and openCARP (Plank et al., 2021) repositories. The original model formulations allow simulating SANC electrophysiology either in basal conditions or under the influence of 1000 nM [ISO]. To consider graded changes in the sympathetic tone, modelling of the β-AR signalling cascade, based on the work of Behar et al. (2016), was adjusted and integrated into these models.

Fig. 1 shows a schematic illustration of the AC-cAMP-PKA signalling cascade after sympathetic stimulation. In general ISO binding to the β-AR or calmodulin activates AC, which transforms ATP into the second messenger molecule cAMP. To model the effect of ISO after stimulation of the β-AR, ATP and cAMP levels were introduced to the model. The increase in cAMP directly affects the hyperpolarisation-activated 'funny' current (I_f) by binding to the ion channel and activating the catalytic subunit of PKA. This leads to phosphorylation of the L-type Ca^{2+} current (I_{CaL}) channel, sodium/potassium pump (I_{NaK}), slow delayed rectifier Kalium (K^+) current (I_{Ks}) channel, ryanodine receptor (RyR) and phospholamban (PLB) regulating the sarcoplasmic/endoplasmic reticulum Ca^{2+}-adenosine triphosphatase (SERCA). The phosphorylation was modelled by the introduction of PKA activity and PLB level, which increased channel conductance values and shifted activation curves.

The Behar–Yaniv (BY) model is based on the Maltsev–Lakatta (ML) rabbit SANC model (Maltsev & Lakatta, 2009) and was extended by adding AC-cAMP-PKA signalling under β-AR stimulation (Yaniv et al., 2015). Due to the different emphasis on the role of Ca^{2+} and membrane clocks, which were discussed in depth earlier, both the ML and BY models are based on a pronounced Ca^{2+} cycling. In contrast the Severi model considers I_f as an additional potent driver of pacemaker function. Therefore the initial parameters and current formulations of the BY and Severi rabbit SANC models differ, which required changes in the signalling cascade prior to integration into the Severi model. Due to a scarcity of experimental data for human SANC, the β-AR signalling cascade was first adjusted and implemented into the Severi (rabbit) SANC model and later integrated into the Fabbri (human) SANC model. The changes detailed here include the introduction of the adjusted cAMP-PKA relationship (eqn (1)). This included a different curve-fitting approach, which was suitable for implementation in the domain-specific modelling language (EasyML) used in openCARP and resulted in slightly different basal PKA activity and cAMP level. Furthermore ATP and PLB levels were added to the models:

$$[\mathrm{PKA}] = \begin{cases} -0.9483 \cdot e^{-[\mathrm{cAMP}]\cdot 0.0656} + 0.9778, & if\ [\mathrm{cAMP}] < 25.87 \\ -0.4526 \cdot e^{-[\mathrm{cAMP}]\cdot 0.0340} + 0.9922, & otherwise \end{cases} \quad (1)$$

More specifically the modulation of the activation gate of I_f followed a Hill-like equation and was adopted from

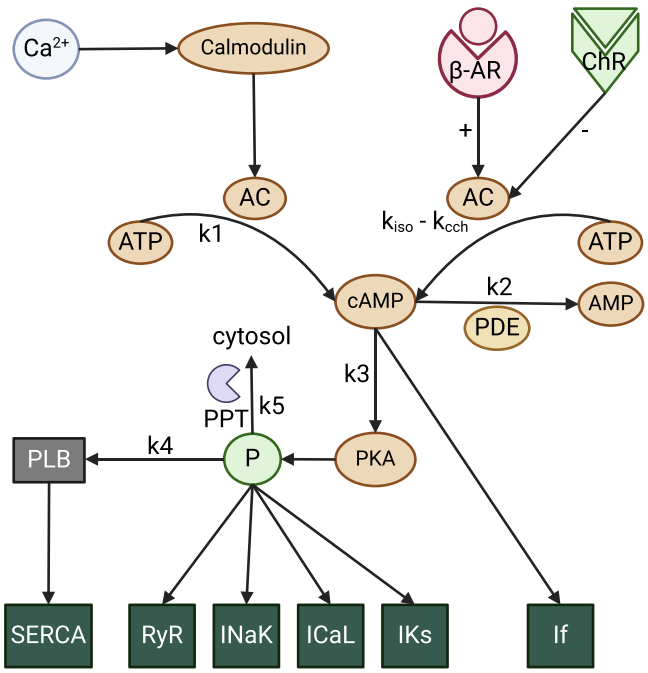

Figure 1. Schematic illustration of the β-adrenergic receptor (β-AR) signalling cascade
Adenylyl cyclase (AC) is activated by β-AR and Ca^{2+}/calmodulin-dependent protein kinase II (CaMKII) and deactivated by cholinergic receptor (ChR) stimulation. Activated AC transforms ATP into second messenger molecule cAMP, which itself activates the catalytic subunit of protein kinase A (PKA). cAMP directly influences the 'funny' current channel (I_f), whereas PKA phosphorylates several targets, including phospholamban (PLB), whose phosphorylation level regulates sarcoplasmic/endoplasmic reticulum Ca^{2+}-adenosine triphosphatase (SERCA). Furthermore two restraining mechanisms regulate the phosphorylation and cAMP levels. Protein phosphatase (PPT) removes phosphate groups from proteins, whereas phosphodiesterase (PDE) breaks phosphodiester bonds of cAMP.

Table 1. β-AR effects on I_f in the different SANC models

I_f	Extended Severi	Extended Fabbri	BY model	Description
	ls $o_{shift} = \frac{K_{if} \cdot [cAMP]^{n_{if}}}{K_{05,if}^{n_{if}} + [cAMP]^{n_{if}}} - 18.76$			Maximal shift of activation by 5.64 mV (Severi) (Behar et al., 2016) and 7.5 mV (Fabbri) (Fabbri et al., 2017)
K_{If}	24.4 mV	26.26 mV	24.4 mV	Maximal I_f activation by cAMP adjusted to maximum increase of 7.5 mV (Fabbri)
$K_{05,If}$	17.33 $\frac{pM}{mg\ protein}$	17.874 $\frac{pM}{mg\ protein}$	17.357 $\frac{pM}{mg\ protein}$	Half-maximal I_f activation of cAMP adjusted to the basal cAMP level

Abbreviations: β-AR, β-adrenergic receptor; BY, Behar–Yaniv; SANC, sinoatrial node cell.

Table 2. β-AR effects on I_{CaL} in the different SANC models

I_{CaL}	Extended Severi	Extended Fabbri	BY model	Description
	ls $o_{inc} = \frac{-0.2152 + K_{ICaL,1} \cdot [PKA]^{10.0808}}{K_{05,ICaL,1}{}^{10.0808} + [PKA]^{10.0808}}$			Maximum increase in amplitude adjusted to a maximum value of 23% and different basal PKA level (Severi et al., 2012) (Fabbri et al., 2017)
$K_{ICaL,1}$	0.4677	0.4707	1.6913	Maximal I_{CaL} activation by PKA adjusted to maximum increase of 23%
$K_{05,ICaL,1}$	0.7213	0.7303	0.8836	Half-maximal I_{CaL} activation of PKA adjusted to the basal PKA level
	ls $o_{shift} = -(\frac{K_{ICaL,2} \cdot [PKA]^{9.281}}{K_{05,ICaL,2}{}^{9.281} + [PKA]^{9.281}} - 18.76)$		Not implemented	Maximum shift of activation by –8 mV, similar to I_f (Severi et al., 2012) (Fabbri et al., 2017)
$K_{ICaL,2}$	27.4444 mV	27.5262 mV	Not implemented	Maximal I_{CaL} activation by PKA adjusted to a maximum shift of –8 mV
$K_{05,ICaL,2}$	0.6535	0.6615	Not implemented	Half-maximal I_{CaL} activation of PKA adjusted to the basal PKA level
	ls $o_{slope} = -1.199 * [PKA] + 1.8526$		Not implemented	Maximum decreased inverse slope of 31%, assumed to be linear (only Severi) (Severi et al., 2012)

Abbreviations: β-AR, β-adrenergic receptor; BY, Behar–Yaniv; PKA, protein kinase A; SANC, sinoatrial node cell.

the BY model (Yaniv et al., 2015). To ensure a similar behaviour between the extended Severi and BY models for the basal concentration of cAMP, the Hill coefficient and a multiplicative factor of the equation were optimised using the *minimise()* function, with sequential least squares programming of the *SciPy* library in Python (Virtanen et al., 2020). The modifications are presented in Table 1.

The level of PKA-dependent phosphorylation modulates I_{CaL} (Trautwein et al., 1987). Thus in the BY model, a maximal I_{CaL} conductance increase of 80% was implemented (Behar et al., 2016). Based on the responses of the original Severi and Fabbri models to 1000 nM [ISO], the modulation of I_{CaL} in the extended models was split into an increase in conductance of 23%, a shift of the activation curve by –8 mV and an inverse slope factor of the activation variable dL_∞ decrease by 31% (only Severi model). The increase in conductance was adjusted by altering the Hill coefficient and the multiplicative factor of the equation, similar to the optimisation of I_f described earlier. The shift of the activation gate was assumed to respond to PKA like the I_f gating variable to cAMP, and the inverse slope factor was assumed to follow a linear decrease. The modifications are presented in Table 2.

In the BY model the PKA-mediated phosphorylation of I_{Ks} and I_{NaK} was not implemented. To balance large increases in the overshoot potential and action potential duration (APD) for high [ISO], the modulation of these two currents was necessary for the extended Severi and Fabbri models. At 1000 nM [ISO] the conductance values of I_{Ks} and I_{NaK} were increased by 20%, whereas only the

Table 3. β-AR effects on I_{Ks} in the different SANC models

I_{Ks}	Extended Severi	Extended Fabbri	BY model	Description
	$Is\ o_{inc} = \frac{-0.2152+K_{/Ks,1}\cdot[PKA]^{10.0808}}{K_{05,/Ks,1}{}^{10.0808}+[PKA]^{10.0808}}$		Not implemented	Maximum increase in amplitude of 20%, similar to I_{Ks} (Severi et al., 2012) (Fabbri et al., 2017)
$K_{/Ks,1}$	0.4333	0.4357	Not implemented	Maximal I_{Ks} activation by PKA adjusted to a maximum increase of 20%
$K_{05,/Ks,1}$	0.7109	0.7042	Not implemented	Half-maximal I_{Ks} activation of PKA adjusted to the basal PKA level
	$Is\ o_{shift} = -(\frac{K_{/Ks,2}\cdot[PKA]^{9.281}}{K_{05,/Ks,2}{}^{9.281}+[PKA]^{9.281}} - 18.76)$		Not implemented	Maximum shift of activation by −14 mV (Severi et al., 2009b), similar to I_f
$K_{/Ks,2}$	34.2549 mV	34.4376 mV	Not implemented	Maximal I_{Ks} activation by PKA adjusted to a maximum shift of –14 mV
$K_{05,/Ks,2}$	0.6955	0.7042	Not implemented	Half-maximal I_{Ks} activation of PKA adjusted to the basal PKA level

Abbreviations: β-AR, β-adrenergic receptor; BY, Behar–Yaniv; PKA, protein kinase A; SANC, sinoatrial node cell.

Table 4. β-AR effects on I_{NaK} in the different SANC models

I_{NaK}	Extended Severi	Extended Fabbri	BY model	Description
	$Is\ o_{inc} = \frac{-0.2152+K_{/NaK}\cdot[PKA]^{10.0808}}{K_{05,/NaK}{}^{10.0808}+[PKA]^{10.0808}}$		Not implemented	Maximum increase in amplitude of 20%, similar to I_{CaL} (Severi et al., 2012) (Fabbri et al., 2017)
$K_{/NaK}$	0.4333	0.4357	Not implemented	Maximal I_{NaK} activation by PKA adjusted to a maximum increase of 20%
$K_{05,/NaK}$	0.7109	0.7042	Not implemented	Half-maximal I_{NaK} activation of PKA adjusted to the basal PKA level

Abbreviations: β-AR, β-adrenergic receptor; BY, Behar–Yaniv; SANC, sinoatrial node cell.

Table 5. β-AR effects on RyR Ca^{2+} release in the different SANC models

koCa	Extended Severi	Extended Fabbri	BY model	Description
	$koCa = koCa_{max}\cdot(RyR_{min} - \frac{RyR_{max}\cdot[PKA]^{n_{RyR}}}{K_{05,RyR}{}^{n_{RyR}}+[PKA]^{n_{RyR}}} - 1)$			RyR phosphorylation (Yaniv et al., 2015)
$K_{05,RyR}$	0.6753	0.6829	0.7	Half-maximal RyR activation of PKA, adjusted to different basal PKA levels

Abbreviations: β-AR, β-adrenergic receptor; BY, Behar–Yaniv; RyR, ryanodine receptor; SANC, sinoatrial node cell.

activation curve of I_{Ks} was shifted by –14 mV. These modulations were assumed to follow a similar Hill curve as I_{CaL}. All changes introduced to I_{Ks} and I_{NaK} are presented in Tables 3 and 4.

The influence of phosphorylation on the Ca^{2+} release by RyR with respect to PKA was modified to compensate for the slightly different basal level of PKA, which was introduced by the new curve-fitting approach. Table 5 presents the introduced changes in the Ca^{2+} release by RyR. The effects on SERCA were implemented phenomenologically and adopted from Behar et al. (2016).

The degradation of PLB phosphorylation was adjusted in both models to ensure a PLB activity level between 0 and 1. Table 6 presents the introduced changes in

Table 6. β-AR effects on PLB degradation in the different SANC models

$diff_{PLBp}$	Extended Severi	Extended Fabbri	BY model	Description
		$k4 = \frac{k_{PLBp} \cdot PKA}{k_{PKA,PLB} + PKA}$		PLB phosphorylation
$k_{PKA,PLB}$	1.5925	1.6103	1.651	Half-maximal PLB phosphorylation
		$k5 = \frac{k_{PP1} \cdot PP1 \cdot PLB_p}{k_{PP1,PLB} + PLB_p}$		Degradation of PLB phosphorylation by protein phosphatase (PPT)
k_{PP1}	$23,575 \frac{1}{\mu M \cdot min}$	$23,850 \frac{1}{\mu M \cdot min}$	$23,575 \frac{1}{\mu M \cdot min}$	Maximal PPT activity
$K_{PP1,PLB}$	0.05967	0.07457	0.06967	Half-maximal PPT activity

Abbreviations: β-AR, β-adrenergic receptor; BY, Behar–Yaniv; PKA, protein kinase A; PLB, phospholamban; SANC, sinoatrial node cell.

Table 7. β-AR effects on cAMP generation in the different SANC models

$diff_{cAMP}$	Extended Severi	Extended Fabbri	BY model	Description
		$k1 = K_{k1} \cdot K_{ACI} + \frac{K_{AC}}{1+e^{\left(\frac{K_{Ca} - \frac{kb_{CM} \cdot fCMi}{kf_{CM} \cdot (1 - fCMi)}}{K_{ACCa}}\right)}}$		Calmodulin-activated AC transforming ATP into cAMP (Yaniv et al., 2015)
K_{k1}	0.92	4.6463	1.0	Factor to compensate for differences in kb_{CM} and kf_{CM}
K_{Ca}	0.09138 μM	0.5640 μM	0.178 μM	Maximal Ca^{2+} adenylyl cyclase activation to compensate for differences in fCMi

Abbreviations: AC, adenylyl cyclase; β-AR, β-adrenergic receptor; BY, Behar–Yaniv; SANC, sinoatrial node cell.

PLB degradation. The phosphorylation of PLB regulating SERCA was implemented based on the experimental data from Vinogradova et al. (2008).

The different Ca^{2+}-related association and dissociation constants (kb_{CM} and kf_{CM}) in the BY and the extended models, along with differences in the fractional occupancy of calmodulin by Ca^{2+} inside the myoplasm (fCMi), required adaptations in the dynamic calculation of cAMP concentration. Therefore the constant defining the maximal AC activation by intracellular Ca^{2+} concentration ($[Ca^{2+}]_i$) (K_{Ca}) was altered in both models, and a multiplicative factor K_{k1} was introduced (Table 7).

Finally compared to the original model formulations published in the CellML repository (https://models.physiomeproject.org/), the location of the conductance increase in I_{CaL} was changed from the total I_{CaL} current to the current components (I_{siCa}, I_{siK} and I_{siNa}) to account for the increase in conductance in the calculation not only of the transmembrane voltage but also of $[Ca^{2+}]_{sub}$ and $[K^+]_i$ (the latter only in the extended Severi model), which was not the case in the original Severi and Fabbri models (Table 8). All model equations, constants and initial values as well as a carputils experiment are provided in the Supporting Information section.

Simulation study

The models were solved using openCARP (Plank et al., 2021) with Rush–Larsen and forward Euler integration schemes for 1000 s, with the last 100 s simulated time considered during analysis. This allowed transient oscillations to equilibrate, resulting in a stable limit cycle. $[Ca^{2+}]_o$ was varied between 0.6 and 1.8 mM with a step size of 0.2 mM, whereas [ISO] ranged from 0 to 10 nM in steps of 2.5 nM, from 10 to 100 nM in steps of 25 nM and 100 to 1000 nM in steps of 250 nM.

To analyse the dominant pacemaking mechanisms that mediate the autonomic regulation via cAMP-PKA signalling, all simulations were performed again, with specific ISO targets modelled as insensitive to phosphorylation, that is, remaining in basal conditions. To assess the relative contribution of the various drivers to BR changes in relation to $[Ca^{2+}]_o$ and [ISO], the main currents were analysed after temporal integration during the AP phases, that is, considering the charge transferred by them during a certain period. Finally for each AP cycle the following markers were calculated: (1) maximum diastolic potential (MDP), defined as the most negative potential during repolarisation; (2) $\max \frac{dV}{dt}$, defined as the maximum of the first-order derivative of the

Table 8. Conductance increase in I_{CaL} multiplied to current components I_{siCa}, I_{siK} and I_{siNa}

$Iso_{inc,cas,ICaL}$	Original Severi/Fabbri	Extended Severi/Fabbri	Description
	$I_{CaL} = (I_{siCa} + I_{siK} + I_{siNa}) \cdot I_{inc,cas,ICaL}$	$I_{CaL} = I_{siCa} + I_{siK} + I_{siNa}$	Sum of I_{CaL} current components
	$I_{siCa} = \frac{2 \cdot P_{CaL} \cdot V}{RTonF \cdot (1 - e^{\frac{-2V}{RTonF}})} \cdot (Ca_{sub} - Ca_o \cdot e^{\frac{-2V}{RTonF}}) \cdot dL \cdot fL \cdot fCa$	$I_{siCa} = \frac{2 \cdot Iso_{increase,ICaL} \cdot P_{CaL} \cdot V}{RTonF \cdot (1 - e^{\frac{-2V}{RTonF}})} \cdot (Ca_{sub} - Ca_o \cdot e^{\frac{-2V}{RTonF}}) \cdot dL \cdot fL \cdot fCa$	Conductance increase in I_{CaL} multiplied to Ca^{2+} current component
	$I_{siK} = \frac{0.000365 \cdot P_{CaL} \cdot V}{RTonF \cdot (1 - e^{\frac{-V}{RTonF}})} \cdot (K_i - K_o \cdot e^{\frac{-V}{RTonF}}) \cdot dL \cdot fL \cdot fCa$	$I_{siK} = \frac{0.000365 \cdot Iso_{increase,ICaL} \cdot P_{CaL} \cdot V}{RTonF \cdot (1 - e^{\frac{-V}{RTonF}})} \cdot (K_i - K_o \cdot e^{\frac{-V}{RTonF}}) \cdot dL \cdot fL \cdot fCa$	Conductance increase in I_{CaL} multiplied to K^+ current component
	$I_{siNa} = \frac{0.0000185 \cdot P_{CaL} \cdot V}{RTonF \cdot (1 - e^{\frac{-V}{RTonF}})} \cdot (Na_i - Na_o \cdot e^{\frac{-V}{RTonF}}) \cdot dL \cdot fL \cdot fCa$	$I_{siNa} = \frac{0.0000185 \cdot Iso_{increase,ICaL} \cdot P_{CaL} \cdot V}{RTonF \cdot (1 - e^{\frac{-V}{RTonF}})} \cdot (Na_i - Na_o \cdot e^{\frac{-V}{RTonF}}) \cdot dL \cdot fL \cdot fCa$	Conductance increase in I_{CaL} multiplied to Na^+ current component

transmembrane voltage; (3) take-off potential (TOP), defined as the transmembrane voltage measured at the time the voltage derivative $\frac{dV}{dt}$ exceeds 0.5 $\frac{mV}{ms}$; (4) APD90, defined as the time of max$\frac{dV}{dt}$ to the point were the AP amplitude repolarised to 90%; (5) DD duration, defined as the time between MDP and TOP; (6) DD early, defined as the first 100 ms after MDP; and (7) DD late, defined as DD without considering the first 100 ms after MDP.

Results

Effects of increased sympathetic tone

The extended Severi model in the basal state yielded a BR of 182 bpm (cycle length (CL) 330 ms), with APD90 and DD shares of 42.1% (138.9 ms) and 45.8 % (151.3 ms), respectively. Based on current integration I_f and the sodium/calcium exchanger current (I_{NaCa}) transferred the most charge during the complete DD. When [ISO] was increased to 10 nM, the BR was elevated by 8.8%, whereas further increases to 100 nM resulted in an elevation of 21.4%. At ∼500 nM a saturation effect was observed with a BR increase of 36.3%, whereas the maximum increase was 36.8% (182–249 bpm) at 1000 nM [ISO]. Selected currents of one complete cycle under basal conditions and the influence of 10 nM [ISO] are shown in Fig. 2*A*,*B*.

Simulations using the extended Fabbri model highlighted interspecies differences. In the basal state the BR was 74 bpm (CL 813 ms), with APD90 and DD shares of 18.4% (149.8 ms) and 76.1% (619.0 ms), respectively. The influence of I_f was attenuated, which rebalanced the pacemaking control towards I_{CaL} and T-type Ca^{2+} channel current (I_{CaT}). The influence of I_{NaCa} remained similar. The transferred charge during the first 100 ms after MDP was similar, with 1.17 and 1.15 pC for the extended Severi and Fabbri models, respectively. The attenuation of I_f during early DD was mainly compensated for by the increased contribution of I_{CaT}. However during late DD the compensation for the reduced contribution of I_f switched to I_{CaL}, with the transferred charge by I_{CaT} already declining due to starting inactivation of the channel.

Because the activation of I_{CaL} was controlled by voltage gates and a Ca^{2+}-activated gate, I_{CaL} largely increased shortly after the elevated cytoplasmic Ca^{2+} concentration caused by the sarcoplasmic Ca^{2+} release of RyR. The delayed Ca^{2+} release extenuated the slope of I_{CaL} and delayed the abrupt downstroke of a main contributor to membrane depolarisation and AP initiation. Because repolarising currents (e.g. I_{Kr}, I_{Ks} and I_{NaK}) were similarly active in both models, the rebalanced contribution, from I_f to I_{CaT} and I_{CaL}, led to a prolonged DD by 467.7 ms. This meant a higher total amount of charge transferred during DD compared to the extended Severi model. Consequently, in the extended Fabbri model, the influence of the Ca^{2+} cycling was increased, the CL was increased and therefore the BR was reduced. In contrast to DD APD90 changed only slightly by 10.9 ms.

Increasing [ISO] to 10 nM elevated the BR by 51.4%, which already exceeded the maximum of the extended Severi model. Further increases of [ISO] to 100 nM

resulted in elevations of 152.7%. Whereas the saturation effect could be observed at ∼250 nM [ISO], with an acceleration of 193.2%, the maximum increase at 1000 nM was 196.2% (74–219 bpm). Fig. 2*C,D* shows selected currents under basal conditions and the influence of 10 nM [ISO] for the extended Fabbri model. Due to the elevated cAMP concentration and PKA activity level, the BR accelerated under sympathetic stimulation. In the case of the extended Severi model, the cAMP level was elevated by 8.0%, whereas PKA activity increased by 3.4%. Similar increases were observed for the extended Fabbri model, with elevations of 8.5% and 3.8%, respectively.

To assess the ion charge transferred between the cell compartments during the complete AP cycle, selected currents were integrated, and the relative contribution to the depolarisation and repolarisation of these currents was calculated. For DD I_{CaL}, I_{CaT}, I_{NaCa} and I_f were considered. The raised cAMP concentration shifted the activation curve of I_f to more positive transmembrane voltages (Hill equation with a maximum of 5.6 and 7.5 mV for 1000 nM [ISO] in the extended Severi and Fabbri models), which opened the voltage gate of the channel earlier during DD and increased the charge transferred during early DD. In the extended Severi model the charge transferred by I_f during early DD was 0.3 pC (28.8% of the charge of the selected currents) in basal conditions and increased to a contribution of 33.8% under the influence of 10 nM [ISO]. For the extended Fabbri model the basal contribution was lower with 0.1 pC (8.5%), with a negligible increase of 0.1% for 10 nM [ISO]. Fig. 3 shows the relative contribution to depolarisation and repolarisation of the selected currents for several [ISO].

The contribution of I_{CaL} during DD was 0.3 and 1.8 pC for the extended Severi and Fabbri models, respectively. For both models the contribution decreased slightly at 10 nM [ISO] by 3.9% and 1.9% (Fig. 3*B,D*). Additionally the charge via I_{CaT} and I_{NaCa} was assessed without being directly affected by the channel phosphorylation. When

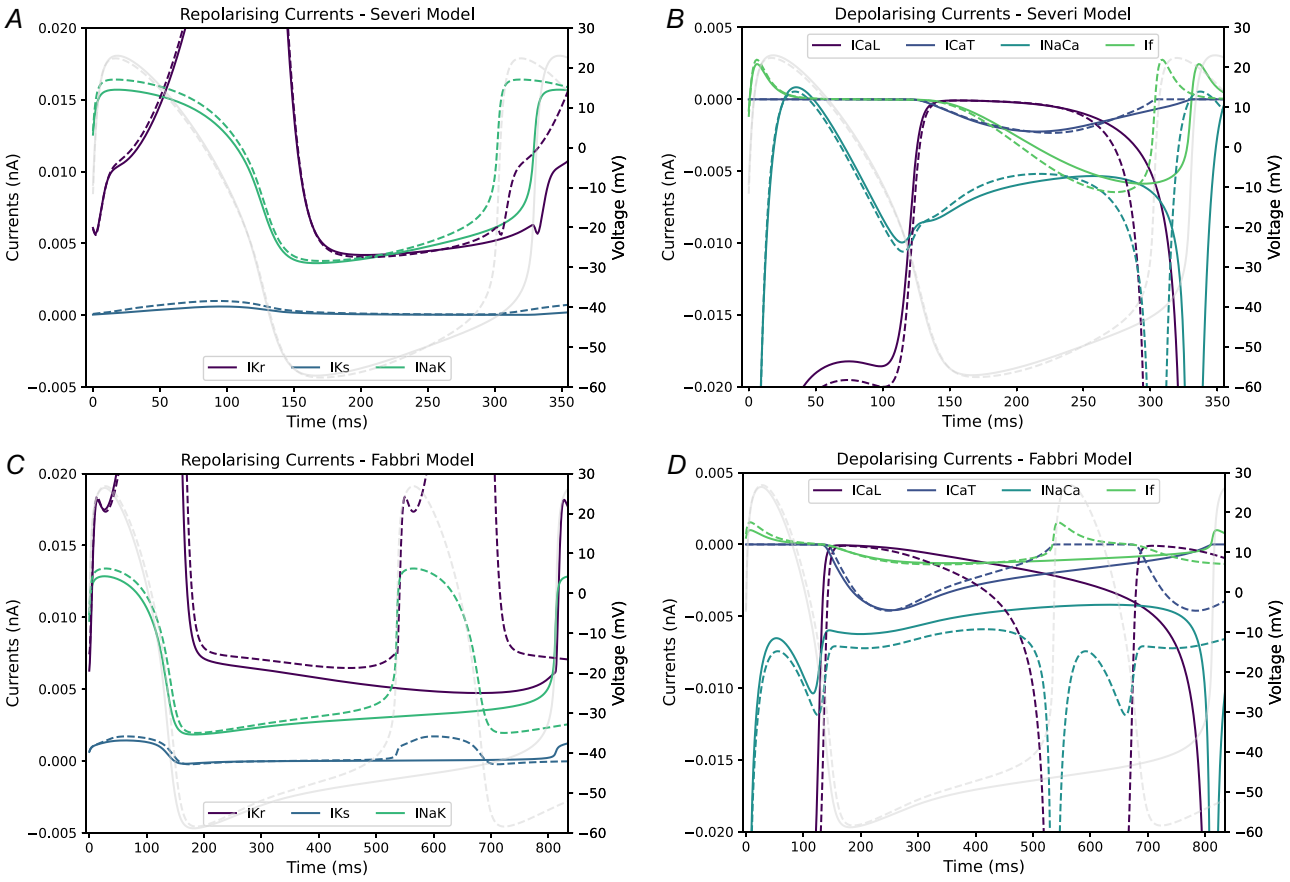

Figure 2.
A, Selected repolarising and *B*, depolarising currents of the extended Severi model during one AP (action potential) cycle under basal conditions (solid) and after β-AR (β-adrenergic receptor) stimulation with 10 nM [ISO] (isoprenaline concentration, dashed). *C*, Selected repolarising and *D*, depolarising currents of the extended Fabbri model during one AP cycle under basal conditions (solid) and after β-AR stimulation with 10 nM [ISO] (dashed). Transmembrane voltage in light grey (background). Note the different scales for depolarising and repolarising currents.

[ISO] was increased to 10 nM in the extended Severi model, the contribution of I_{CaT} with 0.2 pC increased by 1.6%, whereas the impact of I_{NaCa} with 0.9 pC was reduced by 0.2%. In contrast in the extended Fabbri model, the contribution of I_{CaT} with 1.5 pC decreased by 0.8%, and the impact of I_{NaCa} with 3.1 pC was elevated by 3.3%. In the extended Severi model the more pronounced impact of I_f during basal conditions was further increased under β-AR stimulation. In the extended Fabbri model the impact of I_f decreased with increasing [ISO], whereas I_{NaCa} transferred more charge. Although I_{CaL} lost relatively in significance considering the complete DD phase, the activation curve shift and increase in conductance led to an increased contribution in the early part of DD, increasing the depolarisation slope. These results were in accordance with the different emphasis on the membrane and Ca^{2+} clock in both models. However the relatively small changes in current contributions could not fully explain the high interspecies differences observed in the BR increase under β-AR stimulation.

The comparison of further Ca^{2+}-clock phosphorylation targets revealed high variations in the effect on RyR and SERCA, which control the sarcoplasmic Ca^{2+} release and uptake. For 10 nM [ISO] the maximum amplitude of Ca^{2+} release and uptake in the extended Severi model increased by 50.1% and 73.5%, respectively, whereas the maxima in the extended Fabbri model increased by 146.5% and 255.0%. This augmentation of the sarcoplasmic Ca^{2+} exchange resulted in higher I_{NaCa} activity, both during the AP and DD, extruding more Ca^{2+} ions. The sarcoplasmic Ca^{2+} release by the RyR led to a largely increased cytoplasmic Ca^{2+} concentration during

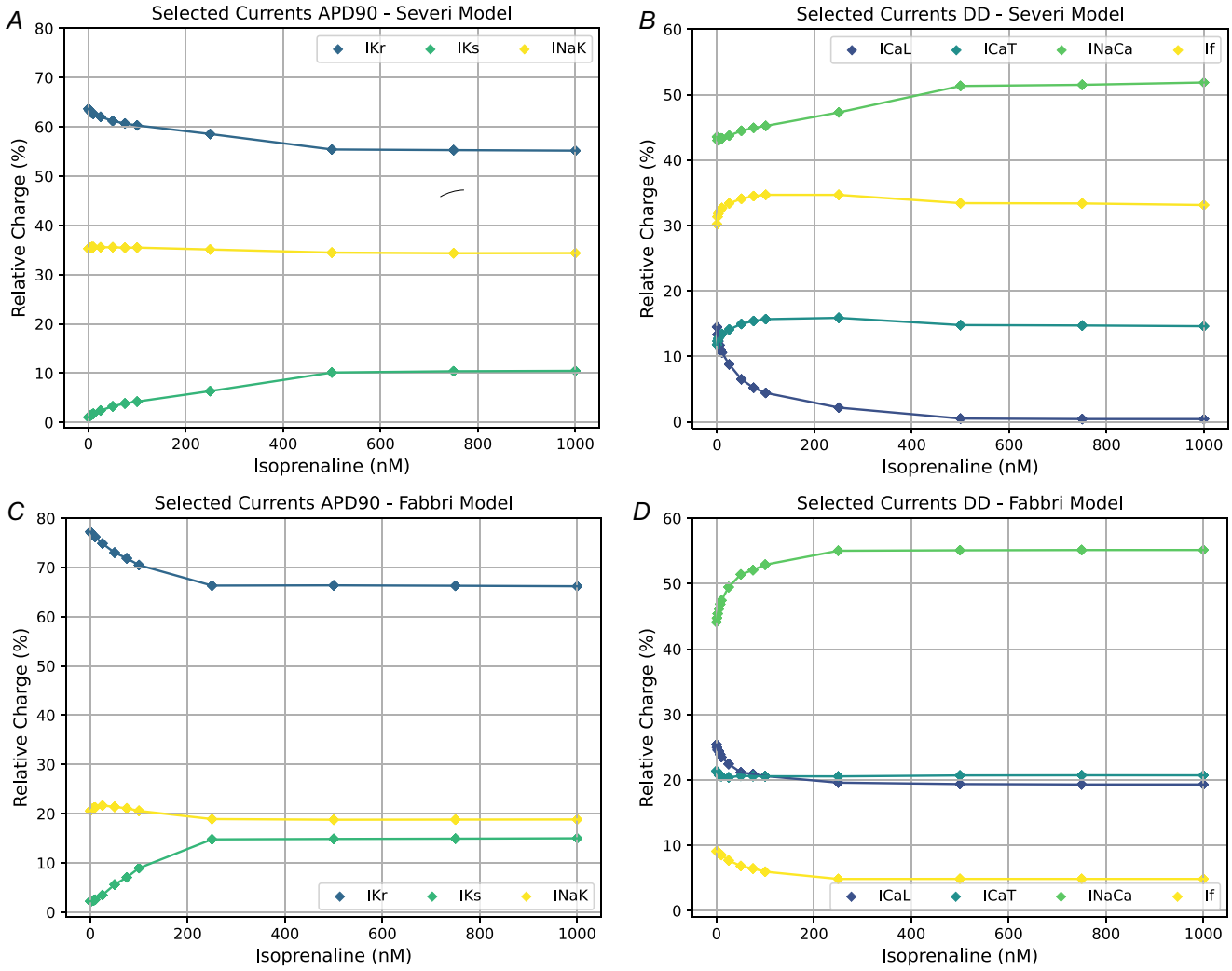

Figure 3.
A, Relative contribution of selected currents to APD90 and *B*, DD (diastolic depolarisation) for different [ISO] (isoprenaline concentration) in the extended Severi model. *C*, Relative contribution of selected currents to APD90 and *D*, DD for different [ISO] in the extended Fabbri model. Note the different scales for the relative charge for APD90 and DD.

DD, which further activated the signalling cascade via calmodulin-stimulated AC and activated I_{CaL} at earlier stages of the DD.

To analyse the currents during the AP, I_{Kr}, I_{Ks} and I_{NaK} were integrated (Fig. 3*A*,*C*). With increasing [ISO] the charge transferred by I_{Ks} increased due to the conductance increase and activation curve shift, whereas the contribution of I_{NaK} remained similar and the contribution of I_{Kr} decreased; 10 nM [ISO] in the extended Severi model yielded slightly elevated contributions of I_{Ks} with 0.1 pC and I_{NaK} with 1.9 pC (0.7% and 0.3% increase, respectively). The contribution of I_{Kr} with 3.3 pC decreased by 1.0%. When [ISO] was further increased to 100 nM, the impact of I_{Ks} increased by 2.4%, whereas the contribution of I_{Kr} and I_{NaK} decreased by 3.4% and 0.1%. Similarly the contribution of I_{Ks} and I_{NaK} in the extended Fabbri model increased slightly for low [ISO], whereas 100 nM [ISO] led to an elevation of I_{Ks} by 6.8%. I_{Kr} was reduced by 6.8%, and I_{NaK} remained similar. The absolute charge of I_{Kr}, I_{Ks} and I_{NaK} increased slightly with elevated [ISO], whereas the decreased contribution of I_{Kr} was mainly counteracted by the largely increased transferred charge through I_{Ks}. This led to the small prolongation of APD90 under β-AR stimulation.

Effects of hypocalcaemia

As previously reported hypocalcaemia leads to lower BRs (Loewe, Lutz, Nairn et al., 2019). For a comparison of the underlying mechanisms responsible for the bradycardic effect, the extended Severi and Fabbri models were analysed for $[Ca^{2+}]_o$ gradually reduced from 1.8 mM (basal conditions) to 1.0 and 1.2 mM, respectively. Even lower $[Ca^{2+}]_o$ could occur in HD patients, but further reductions in $[Ca^{2+}]_o$ led to cessation of automaticity in both SANC models. Ca^{2+} ion fluxes, especially via I_{CaT} and I_{CaL}, largely contribute to the depolarisation of the transmembrane. With the depletion of $[Ca^{2+}]_o$ these ion fluxes decrease due to the smaller concentration gradient. This hampers I_{NaCa}, and depolarisation is compensated by the concurrent repolarising ion fluxes. Thus in case repolarising currents become equal to or larger than depolarising currents, no further AP is initiated. The BR of the extended Severi model decreased by 27.5% (182–132 bpm) for 1.0 mM $[Ca^{2+}]_o$ compared to 1.8 mM, whereas the BR for the extended Fabbri model decreased by 63.5% (74–27 bpm) at 1.2 mM $[Ca^{2+}]_o$. DD was largely prolonged during hypocalcaemia, whereas the APD90 affected the CL prolongation only mildly in each of the models. Again selected currents were integrated to assess the transferred charge during the different phases of the AP. For the extended Severi model the contribution of I_f, with a charge of 0.6 pC in the basal state, was increased by 16.7% for 1.0 mM $[Ca^{2+}]_o$. Consequently the Ca^{2+} cycling was attenuated, and thus, the contribution of I_{CaT} and I_{NaCa} to membrane depolarisation was reduced. Additionally the decreased Ca^{2+} influx attenuated the Ca^{2+} transient as well as the maximum amplitude of the SERCA uptake by 91.6% and release via RyR by 89.0%. Fig. 4 shows the relative contribution to repolarisation and depolarisation of selected currents for several $[Ca^{2+}]_o$. These results are in agreement with previous results of Kohajda et al. (2020), in which a decreased $[Ca^{2+}]_o$ reduced I_{NaCa} and led to a more susceptible DD phase.

In contrast to the extended Severi model, I_{CaL}, I_{CaT} and I_{NaCa} played more important roles in the extended Fabbri model. During early DD I_{CaT} and I_{NaCa} dominated with 0.4 and 0.6 pC, equivalent to a share of 36.7% and 53.1%, whereas I_f and I_{CaL} played a minor role. With decreasing $[Ca^{2+}]_o$ the impact of I_{NaCa} declined and I_f gained influence (Fig. 4*D*). Less extracellular Ca^{2+} decreased the impact of Ca^{2+} in depolarising the membrane. Thus the relative contribution of potassium (K^+) and sodium (Na^+) currents increased. In the basal state the charge transferred during the complete DD mainly consisted of I_{NaCa} with 3.1 pC (44.1%), I_{CaL} with 1.8 pC (25.4%) and I_{CaT} with 1.5 pC (21.4%). On the contrary for decreasing $[Ca^{2+}]_o$, the contribution of I_f and I_{CaL} was elevated by 4.3% and 10.5%, respectively, and the contribution of I_{NaCa} decreased by 10.2% for 1.2 mM $[Ca^{2+}]_o$. The maximum amplitude of the SERCA uptake was attenuated by 68.5%, and the Ca^{2+} release via RyR was reduced by 87.0%.

In general the depolarisation of the membrane depends on the influx and outflux of positively charged ions. In the SANC models this could be either Ca^{2+} ions, which are exchanged between four different cell compartments (intra- and extracellular spaces, junctional and network SR), or K^+ and Na^+, which are exchanged between the intra- and extracellular spaces. The reduction in $[Ca^{2+}]_o$ resulted in slower Ca^{2+} influx through I_{CaT} and I_{CaL} during DD, which in turn led to a slower increase in cytoplasmic Ca^{2+} level and attenuated I_{NaCa} activity as well as Ca^{2+} uptake by SERCA and Ca^{2+} release by RyR. Meanwhile repolarising currents during DD, like I_{Kr}, I_{Ks} and I_{NaK}, were attenuated to a lesser extent, which prolonged the complete depolarisation process to reach TOP and increased I_f based on larger Na^+ and K^+ gradients. Consequently the prolonged DD increased the absolute charge transferred during DD based on the decreased depolarisation slope, whereas the smaller Ca^{2+} uptake was compensated for by an increased I_{NaCa} activity during the APD. Thus the relative contribution of Ca^{2+} ions to membrane depolarisation was slightly reduced, and the relative contribution of I_f, carrying K^+ and Na^+ ions, to reach TOP increased.

Effects of hypocalcaemia and increased sympathetic tone

The influence of graded changes in $[Ca^{2+}]_o$ and [ISO] is shown in Fig. 5. The BR increased largely for small [ISO], whereas the influence of $[Ca^{2+}]_o$ was more linear for higher [ISO]. When the AP cycle was divided into APD90 and DD, in both extended models, a logarithm-like decrease with saturation could be observed for the DD (Fig. 5*C*,*F*). For simulations using the extended Severi model with $[Ca^{2+}]_o$ near the basal conditions, the changes in the APD90 reached a maximum for rather small [ISO] (25–50 nM) (Fig. 5*B*). Decreased $[Ca^{2+}]_o$ led to the attenuation of the maximal effect of [ISO]. For different $[Ca^{2+}]_o$ the BR changes in the extended Fabbri model remained nearly linear. Although the DD was affected similarly, the peak of the APD90 for small [ISO] (25–50 nM) remained prominent while further decreasing $[Ca^{2+}]_o$ extenuated the peak and the total APD prolongation (Fig. 5*E*).

Compensatory effect

Analysing the compensatory effect of ISO during hypocalcaemia showed that for linear decreases in $[Ca^{2+}]_o$ (Fig. 6: dark-turquoise curve), an exponential-like increase in [ISO] (Fig. 6: light-green curve) was needed to maintain the basal BR (Fig. 6: purple curve). In the extended Severi model with $[Ca^{2+}]_o$ of 1.2 mM, 28.0 nM [ISO] restored the initial BR. Although ISO was applied and the basal BR was restored, the charge transferred by the Ca^{2+} transient (CaT) remained smaller, with a decrease of 40.7% compared to basal conditions.

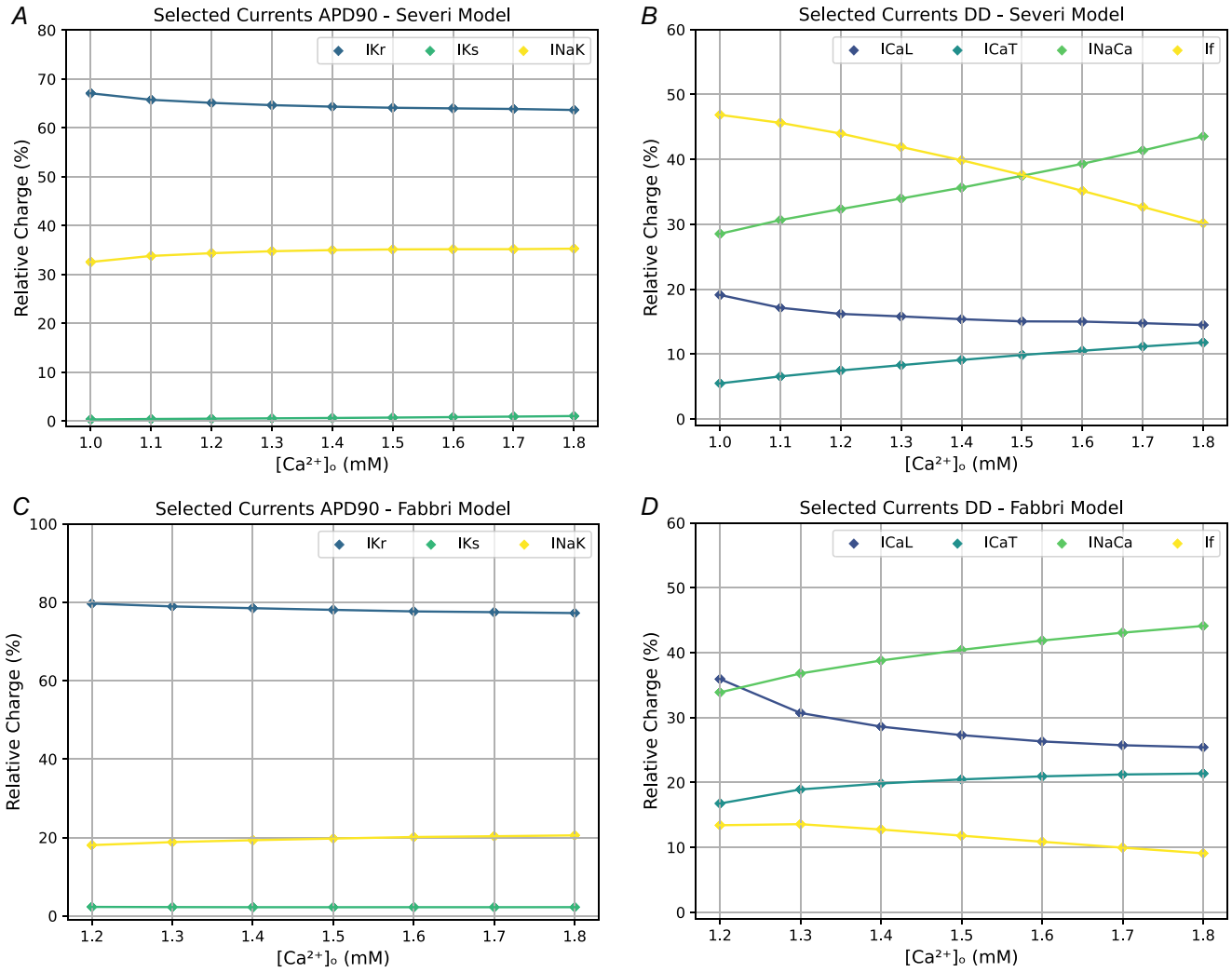

Figure 4.
A, Relative contribution of selected currents to APD90 and *B*, DD (diastolic depolarisation) for different $[Ca^{2+}]_o$ in the extended Severi model. *C*, Relative contribution of selected currents to APD90 and *D*, DD for different $[Ca^{2+}]_o$ in the extended Fabbri model. Note the different scales for the relative charge for APD90 and DD.

Conversely for the Fabbri model 9.6 nM was sufficient, whereas the transferred charge of CaT decreased by 27.8%. This highlighted that the extended Fabbri model is more sensitive not only to changes in $[Ca^{2+}]_o$ but even more so to sympathetic stimulation. Further decreasing $[Ca^{2+}]_o$ to a minimum of 0.6 mM required an [ISO] of 170.0 and 43.6 nM, respectively, to maintain the basal BR. The charge transferred by CaT decreased by 72.9% and 58.8%. Mimicking a sudden loss of sympathetic tone at low $[Ca^{2+}]_o$ ([ISO] dropping to 0 nM after

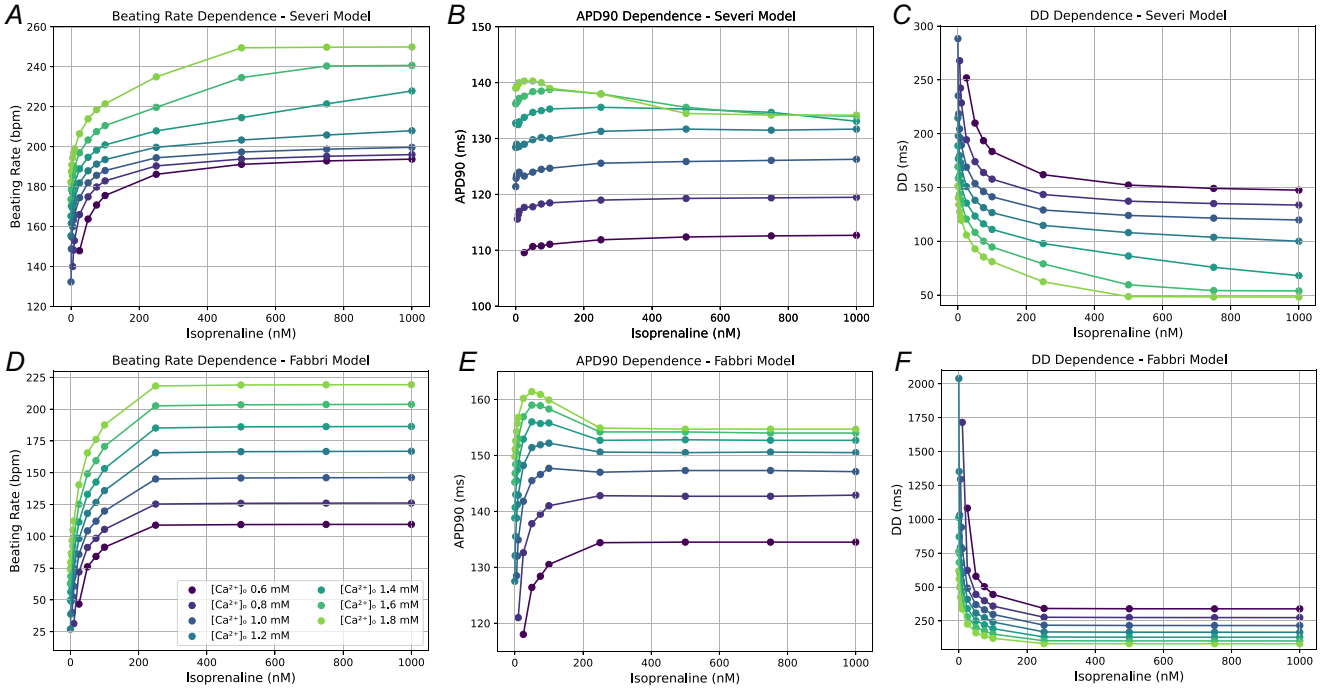

Figure 5.
A, BR (beating rate), *B*, APD90 and *C*, DD (diastolic depolarisation) for varying [ISO] (isoprenaline concentration) and $[Ca^{2+}]_o$ in the extended Severi et al. (rabbit) model; *D*, BR, *E*, APD90 and *F*, DD in the extended Fabbri et al. (human) model. Each line illustrates a different $[Ca^{2+}]_o$.

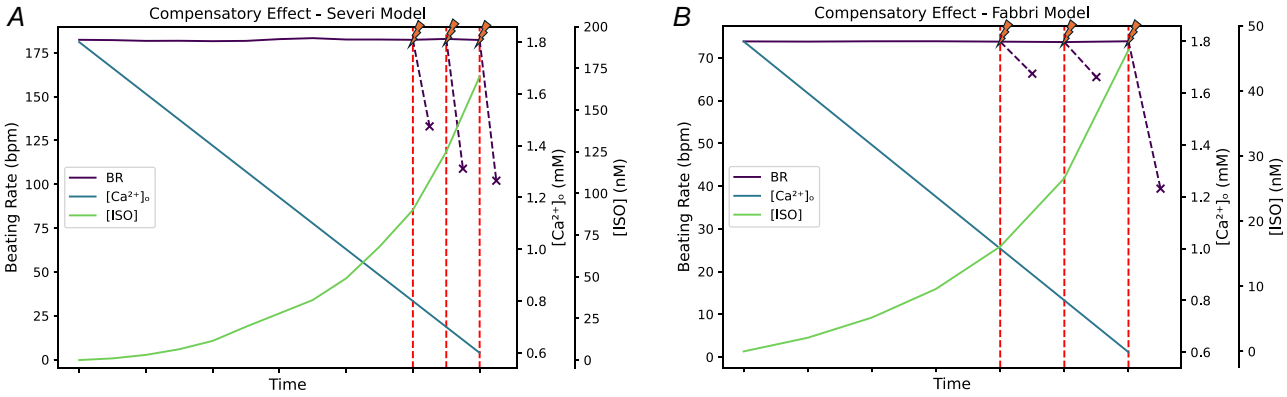

Figure 6.
A, Compensatory effect of ISO (isoprenaline) in the extended Severi model and *B*, in the extended Fabbri model. Several simulations were executed. For each simulation $[Ca^{2+}]_o$ (dark turquoise) was decreased linearly, whereas [ISO] (isoprenaline concentration, light green) was increased to such an extent that it compensated for hypocalcaemia and maintained the basal BR (beating rate, purple). After a stable limit cycle (running the models for 1000 s) was reached, a sudden loss of sympathetic tone was simulated for three different $[Ca^{2+}]_o$ (1.0, 0.8, 0.6 mM) by setting [ISO] to 0 nM abruptly. The sudden loss of sympathetic stimulation is indicated by the flashes and vertical red dashed lines. The purple dashed lines indicate the resulting BRs after a few seconds under the influence of hypocalcaemia in combination with the sudden loss of sympathetic stimulation; 'x' indicates cessation of automaticity.

1000 s) unmasked the low basal BR under hypocalcaemic conditions. In the extended Severi model this led to decreased BRs of 115–130 bpm before automaticity stopped within seconds. Similarly in the extended Fabbri model, cessation occurred after decreased BRs between 39 and 66 bpm. Fig. 6 shows the compensatory effect of ISO and the resulting BRs.

Transferred charge during hypocalcaemia and sympathetic stimulation

Again the AP cycle was divided into APD90 and DD to assess the charge of selected current contributions during these phases. Under basal conditions APD90 was mainly determined by I_{Kr} and I_{NaK} in the extended Severi model. With increased [ISO] I_{Ks} gained influence due to the increase in conduction and activation curve shift, which led to an earlier and prolonged K^+ ion flux duration into the extracellular space (Fig. 7*A*). For decreasing $[Ca^{2+}]_o$ this effect was attenuated.

In the basal state DD was dominated by I_{NaCa} with a contribution of 43.5% and I_f with 30.2%. I_{CaT} and I_{CaL} had smaller shares, with 14.5% and 11.8%, respectively. When [ISO] was gradually increased, the influence of I_f and I_{NaCa} increased, whereas the contribution of I_{CaT} remained similar and I_{CaL} decreased (Fig. 7*B*). When $[Ca^{2+}]_o$ was decreased to 0.6 mM, I_f largely gained in importance, whereas the contribution of I_{CaL}

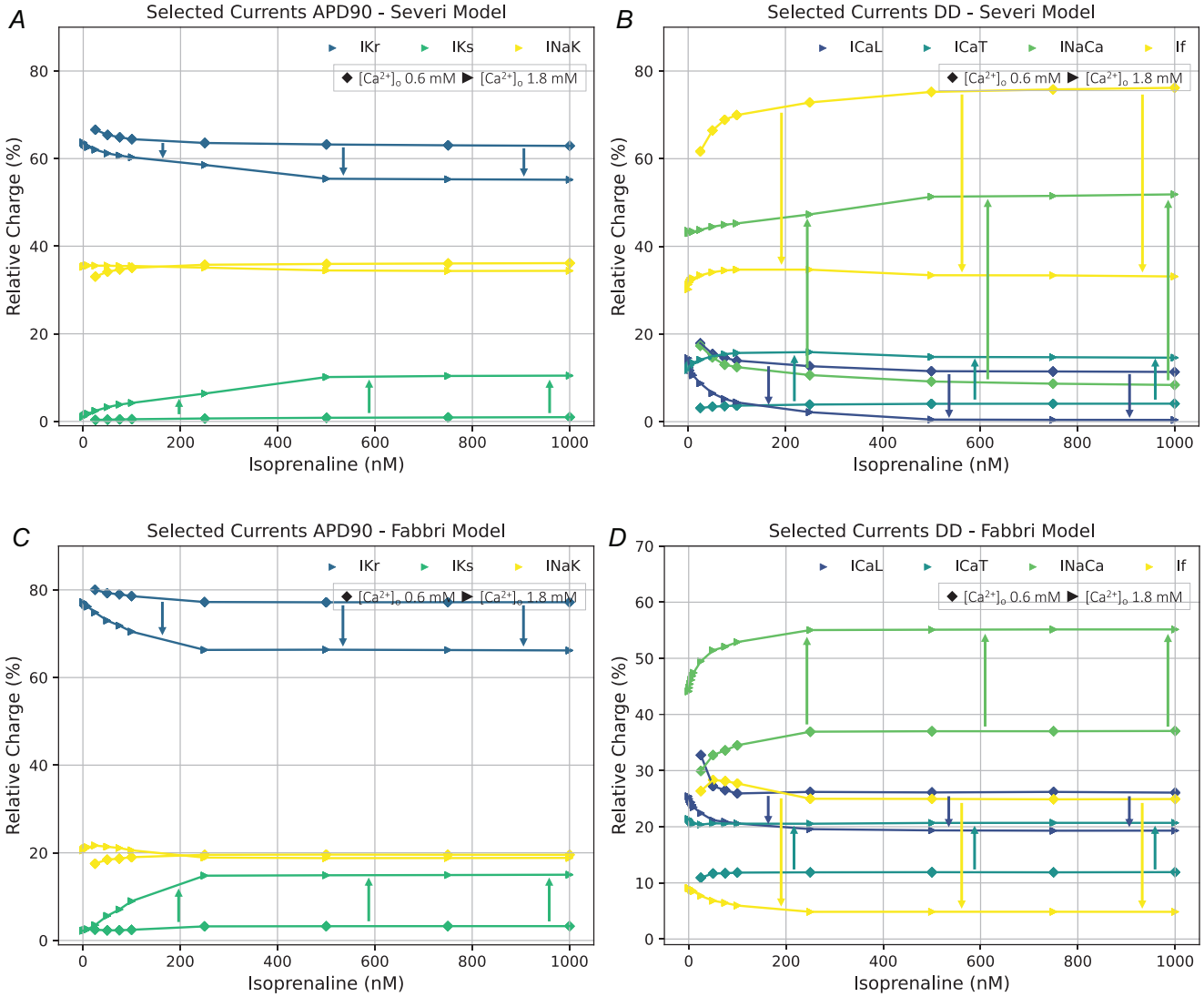

Figure 7.
A, Relative contribution of selected currents to APD90 and *B*, DD (diastolic depolarisation) for different [ISO] (isoprenaline concentration) in the extended Severi model. *C*, Relative contribution of selected currents to APD90 and *D* DD for different [ISO] in the extended Fabbri model. Each symbol represents a different $[Ca^{2+}]_o$. Note the different scales for the relative charge for APD90 and DD.

increased and the influence of I_{CaT} and I_{NaCa} decreased. Consequently the reduced cytoplasmic Ca^{2+} level attenuated the exchange between the cell compartments, which attenuated sarcoplasmic Ca^{2+} uptake and release. Thus the increased conductance and activation curve shift by increased [ISO] on I_{CaL} was negligible during hypocalcaemia.

Comparing these results to the extended Fabbri model, a similar but more pronounced trend for the APD90 could be observed: I_{Kr} dominated for baseline $[Ca^{2+}]_o$ of 1.8 mM and contributed less with increasing [ISO]. In contrast I_{Ks} became more important for reduced $[Ca^{2+}]_o$ and increased [ISO] (Fig. 7*C*).

In basal conditions DD (Fig. 7*D*) was dominated by I_{NaCa}, I_{CaL} and I_{CaT}, with shares of 44.1%, 25.4% and 21.4%, respectively. I_f contributed with only 9.1%. With the gradual increase in [ISO], the influence of I_{NaCa} increased, whereas the impact of I_f and I_{CaL} decreased. The influence of I_{CaT} remained similar.

For both extended models for increased [ISO], the membrane currents and Ca^{2+} cycling were more pronounced, which led to faster depolarisation. Therefore the β-AR stimulation affected both clocks. In contrast the depletion of $[Ca^{2+}]_o$ led to the attenuation of Ca^{2+} influx by I_{CaL} and I_{CaT} due to the smaller gradient between intra- and extracellular spaces. Consequently the reduced cytoplasmic Ca^{2+} level reduced I_{NaCa} as well as the sarcoplasmic Ca^{2+} uptake and release, attenuating the Ca^{2+} transient without directly altering the depolarisation and repolarisation by K^+ and Na^+ ions. Thus for decreased $[Ca^{2+}]_o$ the effect of increased [ISO] switched from ISO-induced increased Ca^{2+} cycling more towards K^+ and Na^+ exchange.

Ion currents underlying the effects of hypocalcaemia and sympathetic stimulation

To assess the predominant mechanisms mediating sympathetic stimulation, numerical simulations, in which only one particular target was altered while the other SR or membrane proteins were modelled as insensitive to PKA phosphorylation and cAMP, were performed. In the extended Severi model at the control $[Ca^{2+}]_o$ of 1.8 mM, the most affected targets for small [ISO] were I_f, I_{CaL} and the Ca^{2+} uptake by SERCA. For 75 nM [ISO] the BR increased by 3.8% in case only the activation curve of I_f was shifted and by 6.0% in case of SERCA phosphorylation. Altering only I_{CaL} increased the BR by 4.4%. In comparison modulating all targets of the ANS at 75 nM [ISO] elevated the BR by 19.8%. For concentrations >100 nM SERCA was the most influential ion flux with a maximum BR increase of 25.8% (Fig. 8*A*, light-green curve).

Decreased $[Ca^{2+}]_o$ augmented the influence of β-AR stimulation. Lower $[Ca^{2+}]_o$ decreased the Ca^{2+} exchange between the cell compartments and, thus, I_f had a stronger influence on pacemaking. ISO affecting only I_f decreased the BR for small [ISO], whereas it increased the BR for higher [ISO]. This effect was more pronounced with lower $[Ca^{2+}]_o$. At 1.4 nM $[Ca^{2+}]_o$ the maximum BR increase for ISO affecting only I_f peaked at 10.3% (Fig. 8*B*, dark-turquoise curve). In case only I_{CaL} was affected by phosphorylation, the impact on the BR peaked at ∼50 nM [ISO], with an elevation of 7.3% (Fig. 8*B*, purple curve). Low $[Ca^{2+}]_o$ led to a more influential I_{CaL}, whereas it attenuated the effect of the Ca^{2+} uptake (Fig. 8*B*, light-green curve). I_{Ks} was more prominent for higher [ISO], still affecting the BR just slightly by 1.0%. The sarcoplasmic Ca^{2+} release via RyR was constant for all [ISO] and I_{NaK}, which was mainly active during APD, and marginally contributed to CL shortening. Fig. 8*A*,*B* summarises the simulation results of the extended Severi model, in which only one target was influenced by [ISO] in basal conditions and $[Ca^{2+}]_o$ of 1.4 mM.

In the extended Fabbri model with basal $[Ca^{2+}]_o$, I_{CaL} was most influential in increasing the BR during sympathetic stimulation. For [ISO] >250 nM affecting only I_{CaL} accelerated the BR by a maximum of 164.9% (Fig. 8*C*, purple curve). Affecting only I_f also influenced pacemaking, peaking at only 13.5% (Fig. 8*C*, dark-turquoise curve). For all other targets the model predicted no significant changes in the BR.

When $[Ca^{2+}]_o$ was gradually decreased the influence of sympathetic stimulation on the BR became larger. For 1.4 mM $[Ca^{2+}]_o$ I_{CaL} remained the most important current, peaking at an increase of 242.0% (Fig. 8*D*, purple curve), whereas the influence of I_f increased to 26.0% during hypocalcaemic conditions (Fig. 8*D*, dark-turquoise curve). Altering all targets led to a maximum increase of 272.0%. Whereas the phosphorylation of the RyR was negligible, all other targets (I_{Ks}, I_{NaK} and SERCA) reduced the BR. Changing only I_{Ks} led to a prolongation of APD due to increased extrusion of K^+ ions during the AP upstroke. Thus for $[Ca^{2+}]_o$ of 1.2 mM, [ISO] >100 nM, the model was not able to reach the TOP anymore and automaticity ceased. This underlined the sensitive interaction between the components of the membrane and Ca^{2+} clock. Thus increased ion fluxes during repolarisation had to be counteracted during depolarisation and vice versa. In case compensation was not possible due to asymmetrically high increases in one of the phases by the alteration of only one target, we observed decreased BRs or cessation of automaticity. Fig. 8*C*,*D* shows the results of the extended Fabbri model under basal $[Ca^{2+}]_o$ of 1.8 mM and hypocalcaemia (1.4 mM), respectively.

Model validation

In basal conditions the extended Severi model yielded a BR of 182 bpm. The BR was higher than that in the original Severi model (169 bpm) and slightly lower than that in the BY model (183 bpm). All basal BRs were inside the physiological range (150–250 bpm) for fresh SANC rabbit cells (Lyashkov et al., 2007). In nearly all sources providing data for several ISO concentrations, elevated [ISO] increased the BR logarithmically. Considering [ISO] of 100 nM the BR increased by 21.3% in the extended Severi, as observed in the *in vitro* experiments (Behar et al., 2016).

Furthermore [ISO] of 300 and 1000 nM resulted in BR elevations of 31.4% and 36.8%, respectively. These predictions are in accordance with the experimental data by Vinogradova et al. (2002). Table 9 summarises the observed BRs in the extended Severi model, several experimental measurements on isolated rabbit SANCs and the effect of increased [ISO] on Langendorff-perfused hearts.

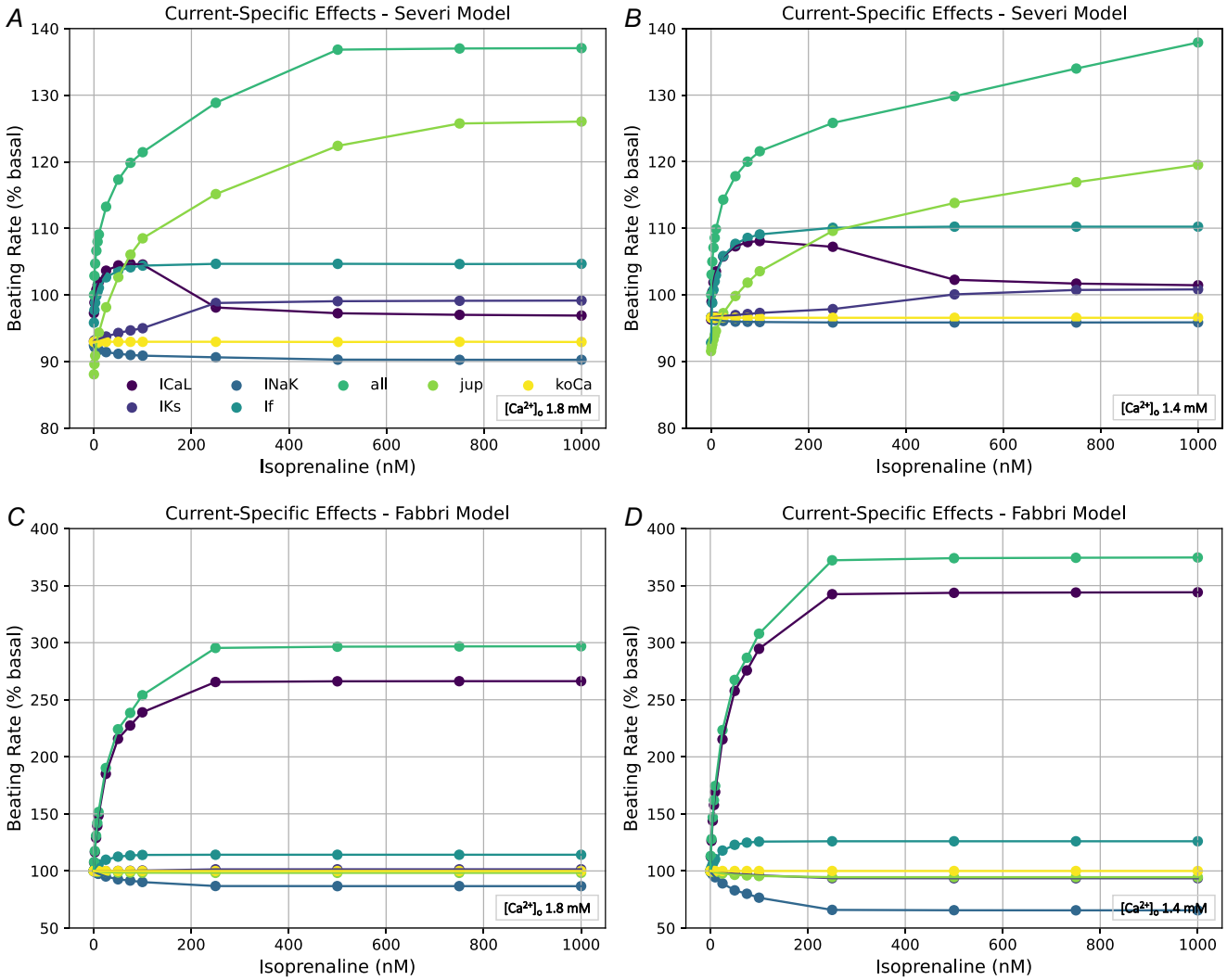

Figure 8.
To assess the predominant mechanisms mediating sympathetic stimulation, numerical simulations, in which only one particular target was altered whereas the other SR (sarcoplasmic reticulum) or membrane proteins were modelled as insensitive to PKA (protein kinase A) phosphorylation and cAMP, were performed. Illustration of ISO (isoprenaline) affecting only one target for control $[Ca^{2+}]_o$ of 1.8 mM (left) and during hypocalcaemia at 1.4 mM (right), with each altered target represented by a different colour. jup and koCa correspond to the SERCA (sarcoplasmic/endoplasmic reticulum Ca^{2+}-adenosine triphosphatase) uptake and a variable mediating the Ca^{2+} release by RyR (ryanodine receptor), respectively. *A*, Extended Severi model for control $[Ca^{2+}]_o$ of 1.8 mM; *B*, extended Severi model for $[Ca^{2+}]_o$ of 1.4 mM; *C*, extended Fabbri model for control $[Ca^{2+}]_o$ of 1.8 mM; and *D*, extended Fabbri model for $[Ca^{2+}]_o$ of 1.4 mM.

Table 9. Effects of different [ISO] on the BR of isolated rabbit SANCs in experimental reports from literature and experiments on Langendorff-perfused hearts (rabbit)

[ISO] (nM)	Extended Severi	Isolated single cells (n = 5, 10)	Langendorff-perfused hearts (n = 5)
0	182 bpm	(150–250) bpm (Lyashkov et al., 2007)	(187.3 ± 10.7) bpm
10	198 bpm, +8.8%	(196.6 ± 34.9) bpm, +7.2% (Behar et al., 2016)	(254.2 ± 44.6) bpm, +35.8%
50	213 bpm, +17.0%	–	(262.7 ± 54.5) bpm, +40.3%
100	221 bpm, +21.4%	(206.2 ± 32.0) bpm, +18.5% (Vinogradova et al., 2002)	(272.5 ± 24.1) bpm, +45.5%
300	239 bpm, +31.3%	(229.5 ± 20.0) bpm, +31.9% (Vinogradova et al., 2002)	–
500	249 bpm, +36.8%	–	(279.1 ± 23.7) bpm, +49.0%
1000	249 bpm, +36.8%	(235.0 ± 52.3) bpm, +35.7% (Vinogradova et al., 2002)	–

Abbreviations: BR, beating rate; [ISO], isoprenaline concentration; SANC, sinoatrial node cell.

Table 10. Effects of concurrent [ISO] and reduced $[Ca^{2+}]_o$ on the BR of Langendorff-perfused hearts (rabbit)

[ISO] (nM)/$[Ca^{2+}]_o$ (mM)	Extended Severi	Langendorff-perfused hearts (n = 5)
0/1.8	182 bpm	(174.3 ± 17.6) bpm
0/0.9	–	(161.6 ± 22.1) bpm, –7.3%
10/0.9	160 bpm, –12.1%	(203.6 ± 32.9) bpm, +16.8%
50/0.9	178 bpm, –2.2%	(209.9 ± 34.9) bpm, +20.4%
100/0.9	185 bpm, +1.6%	(242.9 ± 17.6) bpm, +39.4%
500/0.9	195 bpm, +7.1%	(248.1 ± 19.9) bpm, +42.3%

Abbreviations: BR, beating rate; [ISO], isoprenaline concentration.

The concurrent effects of hypocalcaemia (0.9 mM $[Ca^{2+}]_o$) and different [ISO] on the BR are presented in Table 10. As under basal $[Ca^{2+}]_o$ the β-AR response under hypocalcaemia was less pronounced in the extended Severi model than in the Langendorff-perfused heart experiments. Comparing the ranges of BR increase revealed differences in the response to sympathetic stimulation under hypocalcaemic conditions. The extended Severi model did not initiate APs at 0.9 mM $[Ca^{2+}]_o$ without ISO stimulation. Meanwhile the Langendorff-perfused hearts exhibited a BR decrease of 7.3%. [ISO] elevated to 10 nM led to a BR decrease of 12.1% in the extended Severi model and an increase of 16.8% in experimentally obtained BR. Further increasing [ISO] under hypocalcaemia led to a logarithmic-like increase in the BR for both the extended Severi model and the Langendorff-perfused hearts. However the BR increase started to saturate faster in the extended Severi model, highlighting that the model was more affected by $[Ca^{2+}]_o$ than that observed in the Langendorff-perfused heart experiments.

Furthermore [cAMP] ranged from 21.09 to 88.94 and 19.73 to 101.78 pM/mg protein in the extended Severi and Fabbri models, respectively, whereas the PKA activity increased from 0.74 to 0.97 and 0.72 to 0.98 in the extended Severi and Fabbri models, respectively. In comparison [cAMP] in the BY model ranged from 20.04 to 103.94 pM/mg protein, whereas PKA increased from 0.74 to 0.97 (Behar et al., 2016).

Discussion

This study analysed the interspecies differences in the SANC response to hypocalcaemia (Loewe, Lutz, Nagy et al., 2019), β-AR stimulation and the combination of both mechanisms, that is, the compensation for hypocalcaemia-induced bradycardia by the ANS, in extended computational models of rabbit (Severi) and human (Fabbri) SANCs. The analysis of the results revealed the following. (1) In the extended Severi model the primary pacemaker currents during DD were I_f and I_{NaCa}, whereas for the extended Fabbri model, pacemaking was rebalanced towards I_{CaT}, I_{CaL} and I_{NaCa}. (2) The integration of the β-AR signalling cascade increased the Ca^{2+} inflow and cycling during DD (I_{CaL}, SR Ca^{2+} uptake and release directly, and I_{CaT}, I_{NaCa} indirectly) and thus shortened DD and CL. (3) A reduction in $[Ca^{2+}]_o$

resulted in decreased Ca^{2+} inflow and cycling (I_{CaT}, I_{CaL}, SR Ca^{2+} uptake and release), prolonging DD and CL. (4) Hypocalcaemia is compensated for by an increased sympathetic tone because similar targets were affected by both mechanisms. (5) The extended Fabbri model was more sensitive to sympathetic stimulation and hypocalcaemia as transmembrane depolarisation by Ca^{2+} is more accentuated, and small current variations generally have a larger effect on slower DD phases than on faster ones. Zaza and Lombardi (2001) analysed the influence of small current variations on increased DDs in SANCs, and Winter and Shattock (2016) discussed the impact of small current variations on increased APDs in ventricular myocytes. These geometrical considerations could also be applied to the prolonged DD phase in the extended Fabbri SANC model.

Interspecies differences under basal conditions

In the past there was different emphasis on the role of Ca^{2+} cycling *versus* the contribution of I_f. Despite a detailed description of intracellular Ca^{2+} cycling, I_f and I_{NaCa} were the primary pacemaker currents in the original Severi model. In the original Fabbri model the impact of I_f was attenuated, which rebalanced the pacemaking control more towards $I_{CaT,}$ I_{CaL} and I_{NaCa}. This remained similar in the extended models. Thus in the extended Fabbri model, the reduced contribution of I_f (compared to the extended Severi model) during early DD was primarily compensated for by the increased impact of I_{CaT}. During late DD the compensation for the decreased contribution of I_f shifted towards I_{CaL}, with the charge transferred by I_{CaT} declining due to channel inactivation. Because the activation of I_{CaL} was controlled by voltage and Ca^{2+}-activated gates, most charge was transferred shortly after the Ca^{2+} gate was opened by an increase in cytoplasmic Ca^{2+} concentration, which was caused by sarcoplasmic Ca^{2+} release from RyR. Delayed sarcoplasmic Ca^{2+} release attenuated the slope of I_{CaL} and delayed the rapid downstroke of a major contributor to reaching TOP and initiating the AP upstroke. Because repolarising currents (e.g. I_{Kr}, I_{Ks} and I_{NaK}) were similarly active in both models, the different contributions during DD led to a prolonged depolarisation phase and greater total charge transferred during DD compared to the extended Severi model. As a result in the extended Fabbri model, the impact of Ca^{2+} cycling was amplified, the CL was prolonged and thus the BR was reduced.

Logarithmic BR increase under sympathetic stimulation

By integrating the β-AR signalling cascade of Behar et al. (2016) into both models, continuous modelling of β-AR effects on critical membrane (I_{CaL}, I_f, I_{Ks}, I_{NaK}) and SR (Ca^{2+} release by RyR and uptake by SERCA) currents was enabled. Increases in [ISO] led to an increased cAMP and PKA activity level, which affected the coupled clock mechanisms, elevating the BR. For increased ISO >500 and 250 nM, for the extended Severi and Fabbri models, respectively, a saturation effect was observed. This was consistent with the implementation of the conductance increases and activation curve shifts as Hill curves.

The comparison of sympathetic stimulation affecting the BY and extended Severi rabbit SANC models revealed that the extended Severi model predicted a stronger maximal response to β-AR stimulation on the BR (+36.8%) than the BY model (+22.0%). Whereas the BY model closely reproduced the experimental data of cultured SANCs conducted by Yaniv et al. (2015), several studies implied larger BR increases (Bucchi, 2003; Barbuti et al., 2007; Bucchi et al., 2007: Vinogradova et al., 2008) and slower saturation effects with respect to autonomic stimulation by elevated [ISO] (Vinogradova et al., 2002). Yang et al. (2012) analysed the differences between fresh and cultured rabbit SANCs. The results suggested that cultured SANCs underlay a partial disengagement of the coupled clock mechanisms. Whereas the reduction in PKA-dependent phosphorylation of PLB and RyR was partly restored by increased β-AR stimulation (1 nM [ISO]), the phosphorylation of further critical surface membrane channels, such as I_{CaL}, I_{Ks} or I_{NaK}, was not assessed and might also be affected. Because the parametrisation of the BY model was based on cells cultured for 48 h, with 1 nM [ISO] referring to basal conditions to counteract the decreased BR, the maximal effect of the ANS might also be attenuated. The logarithmic BR increase, in combination with the restoration of the uncoupling effects of PLB and RyR, could explain the discrepancy between the experimental data of cultured and fresh SANCs and the different BR increases in the BY model compared to the extended Severi model. Additional differences between both rabbit models were mainly based on the different $[Ca^{2+}]_o$ used as basal conditions (2.0 mM BY *vs.* 1.8 mM Severi models) and differently weighted contributions of the membrane and Ca^{2+} clock. Like its parental model the extended Severi model emphasises I_f as a main contributor to the membrane clock, whereas the BY model focuses on a more pronounced Ca^{2+} cycling.

It could be further argued that even the maximum BR increase of 36.8% in the extended Severi model was still underestimated when considering the maximum BR increase of 49.0% in the Langendorff-perfused hearts for 500 nM [ISO]. This might be caused by the isolation process and, thus, the reduced number of channels, receptors, or the uncoupling of β-AR signalling cascade components, which attenuated the β-AR cell response. Nevertheless the logarithmic BR increases with saturation

were observed for single-cell and Langendorff-perfused heart experiments.

The literature review on human SANCs revealed an even greater scarcity of experimental data. Tsutsui et al. (2018) analysed the response of four human SANCs to a maximum of 1000 nM [ISO], observing a relative BR increase of 42.8% (35–50 bpm). However due to significant differences between the basal BRs of the experimental data and the basal BR of the Fabbri model and the lack of experimental data on ISO effects on specific target currents, pumps and exchangers, the β-AR response in the Fabbri model was not modelled to a maximum increase of 42.8%. Instead the ISO-related effects on the target currents, pumps and exchangers were adapted from the extended Severi to the extended Fabbri models.

Ion currents underlying the effects of hypocalcaemia and sympathetic stimulation

In the extended Severi model modulation of I_f by ISO alone resulted in a maximum BR increase of 4.4%. This emphasised the dominant role of I_f in mediating the chronotropic effect under autonomic regulation. Therefore I_f increased the steepness of the DD slope near the MDP, which shortened the depolarisation of the membrane during early DD. In contrast to affecting one of the other targets, only the phosphorylation of SERCA was more pronounced for high [ISO], with a maximum BR elevation of 25.8%. This increased the Ca^{2+} uptake and resulted in an increased sarcoplasmic Ca^{2+} release by RyR, which increased I_{CaL} and I_{NaCa}. Thus the depolarisation slope was steeper, which shortened DD significantly.

Augmenting only I_{CaL} led to increased BRs for small and the inverse effect for high [ISO]. The modulation of I_{CaL} resulted in a shortened late phase of the DD and increased upstroke velocity of the AP. The inverted effect was based on larger Ca^{2+} ion transport through an increase in conductance and activation curve shift. Thus the time during which positively charged ions entered the cytoplasm during late DD and the early stages of the AP upstroke was prolonged. Without subsequent elevations in SERCA and I_{NaCa} activity, a largely increased Ca^{2+} influx prolonged the repolarisation and, thus, the CL.

The phosphorylation of sarcoplasmic Ca^{2+} release by RyR prolonged the CL for small [ISO], whereas larger [ISO] slightly decreased the CL. Thus the predictions of the extended Severi model regarding the critical role of Ca^{2+} uptake by SERCA align with the findings of Itzhaki et al. (2011), who demonstrated the significance of SERCA-mediated Ca^{2+} reuptake into the SR in human-induced pluripotent stem cell-derived cardiomyocytes.

Similarly I_{Ks} elevated the BR for increasing [ISO]. By shifting the voltage-dependent activation curve, the K^+ ion channel gates opened and at lower voltages, which, in combination with the increased maximum current amplitude, led to a faster repolarisation and moderate shortening of the APD. Instead introducing conductance increases only in I_{NaK} yielded APD prolongations, which slightly increased the AP CL. Compared to I_{Ks} this meant that the heightened K^+ influx without the ion channel opening earlier in time, based on an activation curve shift, led to a prolonged time of K^+ extrusion, which increased the APD.

Based on the lack of experimental data, the PKA-mediated modulation of I_{Ks} and I_{NaK} was not included in the BY model implementation. However omitting the influence of I_{Ks} in the extended Severi model led to BRs peaking at 100 nM [ISO]. Besides when [ISO] was further increased, the BR decreased, which was caused by increased APD and AP upstroke. The influence of I_f in the extended Severi model in combination with the cAMP-induced activation gate shift without subsequent modulations in I_{Ks}, extruding K^+ ions during the APD, resulted in non-physiological prolongations. On the contrary, omitting the phosphorylation of only I_{NaK} increased the BR to values higher than those observed in experiments (maximum of +44.1% BR increase). To balance the increased K^+ ion extrusion introduced by I_{Ks}, an increase in I_{NaK} was necessary to obtain simulation results in line with the experimental data from isolated single cells.

In the extended Fabbri model in which pacemaking was rebalanced towards I_{CaT} and I_{CaL}, modulating only I_{CaL} with the other β-AR targets remaining unchanged largely influenced the BR. Because Ca^{2+} cycling between the cell compartments was more pronounced in basal conditions, SERCA and I_{NaCa} were able to extrude the increased amount of Ca^{2+} ions under ANS stimulation without prolonging the CL, as was the case in the extended Severi model.

If only I_f was modulated the activation curve shift resulted in an earlier opening of the channel, but the decreased impact of I_f influenced the BR acceleration less pronounced. With decreasing $[Ca^{2+}]_o$ the contribution of I_f increased, which was caused by the relatively elevated significance of K^+ and Na^+ fluxes in depolarising the membrane, whereas the Ca^{2+} cycling lost significance. The reduced $[Ca^{2+}]_o$ attenuated I_{CaT} and I_{NaCa} and, thus, the cytoplasmic Ca^{2+} content, which subsequently attenuated the sarcoplasmic Ca^{2+} uptake and release by RyR.

Whereas at $[Ca^{2+}]_o$ near the basal conditions, augmenting only I_{Ks} had negligible effects, the alteration of I_{NaK} slightly elevated the BR. At 1.2 mM $[Ca^{2+}]_o$ the BR decreased and prevented AP generation for higher [ISO]. In both cases this originated from the elevated K^+ and

Na^+ exchange between the intra- and extracellular spaces at low $[Ca^{2+}]_o$. Without simultaneous counteraction APD was prolonged, and repolarisation of the transmembrane was prevented.

Similarly in the basal state modulating only the SERCA uptake resulted in negligible BR changes, whereas for reduced $[Ca^{2+}]_o$, the CL was prolonged slightly. Under extreme hypocalcaemic conditions the reduced Ca^{2+} uptake inhibited the release by the RyR and the activation of I_{CaL} and I_{NaCa} caused by the reduced $[Ca^{2+}]_i$. Thus the DD was prolonged, initiating the AP upstroke later. Again this highlighted the critical role of the SERCA uptake, inhibiting the Ca^{2+} release by the RyR and the tightly controlled Ca^{2+} balance of the different compartments influencing each other (Itzhaki et al., 2011).

Contrary to the extended Severi model, the attenuation of I_f resulted in reduced K^+ and Na^+ ion exchanges between the extra- and intracellular spaces, which also extenuated K^+ and Na^+ ion transfer to maintain homeostasis via I_{Ks} and I_{NaK}. Instead the Fabbri model was based on a more pronounced Ca^{2+} exchange between the different cell compartments, especially Ca^{2+} influx from the extracellular space by I_{CaT} and I_{CaL}. Consequently the sarcoplasmic Ca^{2+} uptake by SERCA and release by RyR were elevated. In combination with the increases in Ca^{2+} cycling components caused by phosphorylation, this led to higher sensitivity with respect to β-AR stimulation.

The simultaneous occurrence of cAMP-mediated gate shifting and phosphorylation of the membrane and SR targets exerted the largest effect on the BR in both extended SANC models. To achieve a reduction in the entire CL, the elevated ion exchanges during depolarisation needed to be compensated for by increased currents during repolarisation and vice versa. Thus the intricately orchestrated interplay by the membrane and Ca^{2+} clock could increase the resulting BR. This involved an earlier initiation and steeper DD slope, facilitated by the activation curve shift of I_f, coupled with increased Ca^{2+} cycling through augmented I_{CaL}, sarcoplasmic Ca^{2+} uptake and release. Consequently the DD phase was rapidly shortened, whereas the APD remained akin to the basal conditions. A prolongation of the APD was prevented by the increased repolarisation currents I_{Ks} and I_{NaK}.

Hypocalcaemia-induced BR reduction

Loewe, Lutz, Nairn et al. (2019) analysed the effects of altered electrolyte levels in a modified version of the Fabbri et al. human SANC model. The changes included the introduction of variable $[K^+]_i$ and $[Na^+]_i$ to reflect conditions in HD patients more realistically. Whereas these alterations impaired the response to sympathetic stimulation, the results indicated that hypocalcaemia markedly impairs pacemaking, and alterations in the $[K^+]_o$ and $[Na^+]_o$ levels yielded negligible and mild effects on the BR, respectively. Therefore hypocalcaemia-induced slowing of the sinus node pacemaking increased the total CL for both rabbit and human SANC models. The reduction in $[Ca^{2+}]_o$ attenuated the amount of Ca^{2+} ions entering the cell from the extracellular space, which also reduced the intracellular Ca^{2+} cycling. Therefore I_{CaT}, I_{CaL}, I_{NaCa}, the Ca^{2+} uptake by SERCA and the release by RyR were decreased, whereas the contribution to the depolarisation of I_f was increased. Due to the larger impact of I_f, pacemaking in the extended Severi model was less sensitive regarding hypocalcaemia, which resulted in smaller CL increases compared to the extended Fabbri model.

An increased sympathetic tone compensates for hypocalcaemia

Assessing the compensatory effect of the ANS with respect to hypocalcaemia-induced bradycardia, typically occurring in HD patients, both rabbit and human models predicted that reduced $[Ca^{2+}]_o$ can be compensated for to a certain extent by an increased sympathetic tone. Stary et al. (2023) implemented a linear [ISO] dependence in the Fabbri model, which affected the BR almost linearly. Contrary to these findings the integration of the non-linear β-AR signalling cascade led to a logarithmic increase with saturation of the BR. This was similarly observed in several experiments on isolated rabbit SANCs (Vinogradova et al., 2002) (Behar et al., 2016) as well as the Langendroff-perfused heart experiments. Furthermore this was in accordance with the continuous implementation of the sympathetic effects on critical membrane and SR currents, as Hill functions. Thus the stimulation modulated the targets nearly linearly close to the basal conditions, with a saturation effect for more pronounced changes. The combination of both hypocalcaemia, which attenuated the Ca^{2+} cycling, and the β-AR stimulation, which increased the influence of six different targets (I_{CaL}, I_f, I_{NaK}, I_{Ks}, RyR and SERCA), revealed that three of these targets were directly affected by $[Ca^{2+}]_o$ depletion and increased conductance and activation curve shifts by the ANS. Thus hypocalcaemia-induced attenuations of the Ca^{2+} cycling were directly neutralised by an increased sympathetic tone. With less Ca^{2+} available the increasing effects needed to be more pronounced to restore the basal BR. The other three modulated β-AR targets controlled the exchange of K^+ and Na^+ in the intra- and extracellular spaces. The combination of the attenuated I_f in the extended Fabbri model, with the increased impact of the Ca^{2+} clock components in regulating the BR, explained

the higher sensitivity of the extended Fabbri model towards hypocalcaemia and β-AR stimulation.

Verkerk and Wilders (2023) discussed changes in the kinetics of I_{Ks} with respect to β-AR stimulation in human SANCs. Based on the experimental data using HEK-293 cells, the K^+:Na^+ permeability, conductance and reversal potential were adjusted. Including these findings in the extended Fabbri model reduced the basal BR slightly to 70 bpm and the ISO-induced BR acceleration to a maximum of 191 bpm (+171.7%) in the case of stimulation with 1000 nM ISO. It can be argued that the increased BR of 191 bpm is closer to the physiologically achievable maximum of an adult human (maximum heart rate of an adult is ∼220–age bpm on average; American Heart Association, 2024) than the 219 bpm obtained using the I_{Ks} formulation of the original Fabbri model. Additionally the complete integration of the cholinergic receptor stimulation could further enhance the extended models towards more realistic predictions. This could include simulations with a sudden increase in the parasympathetic tone.

Limitations

During the integration process of the β-AR signalling cascade into the SANC models, some assumptions were made due to the scarcity of experimental data. Because the generation and degradation of intracellular cAMP are influenced by several model parameters, these equations were adjusted to cover the interspecies differences. Besides the PKA-dependent activation curve shift of I_{CaL} and I_{Ks} was expected to behave similar to the cAMP-mediated activation curve shift of I_f. Finally the increase in conductance values for I_{NaK} and I_{Ks} was assumed to be similar to the PKA-mediated phosphorylation of I_{CaL}. To ensure a more realistic sympathetic stimulation, channel-specific differences in reference to changes in the PKA level should be further investigated. Although the Fabbri model was derived from the Severi model and thus validated in the work of Fabbri et al. (2017), interspecies differences in the adrenergic cell response, for example, mentioned by MacDonald et al. (2020), do not allow for complete validation of the extended Fabbri model based on the currently limited experimental data.

Furthermore the compensatory effect was evaluated under isolated sympathetic stimulation with varying [ISO]. Due to the highly non-linear nature of the models, the simultaneous sympathetic and parasympathetic stimulations, characterised by high [ISO] and [ACh], are unlikely to affect the BR in the same manner as low [ISO] in the absence of [ACh]. This phenomenon, known as accentuated antagonism, was also identified in the experiments of Levy (1971) and is represented in the BY model (Behar et al., 2016).

Loewe, Lutz, Nairn et al. (2019) extended the Fabbri model to simulate variable $[K^+]_i$ and $[Na^+]_i$ with a constant basal sympathetic tone. These optimisations also resulted in more stability towards lower $[Ca^{2+}]_o$. Further decreases in the Ca^{2+} levels in combination with lower [ISO] as well as variable K^+/Na^+ formulations might also be of interest to uncover the pathogenesis of hypocalcaemia-induced bradycardia. The original and extended Severi model implementation contained variable $[Na^+]_i$. However fixing $[Na^+]_i$ to 7.5 mM (initial value) to ensure similarity of $[Na^+]_i$ formulation altered the simulation results negligibly. The effect of ISO increased marginally for small and decreased for high [ISO]. To improve the models towards more realistic effects of changes in electrolyte levels, variable $[K^+]_i$ and $[Na^+]_i$ should be implemented in both extended models.

Moreover automaticity was assessed only on single-cell level. To capture the excitation initiating the heartbeat *in vivo*, complementing the simulations on single-cell level with tissue patches of coupled SANCs and including the surrounding myocardium are necessary (Amsaleg et al., 2022). Furthermore the experimental results of the Langendorff-perfused hearts indicated higher sensitivity towards increased [ISO] compared to single-cell experiments. However the modulations of specific membrane and SR channels are modelled based on isolated single-cell experiments and, thus the resulting conductance increases, and activation curve shifts should be complemented by experiments with Langendorff-perfused hearts.

It is also worth mentioning that both SANC models by Severi et al. and Fabbri et al. were derived based on patch-clamp experiments on isolated single cells in Tyrode solution. Unfortunately as Severi et al. pointed out, the $[Ca^{2+}]_o$ of standard Tyrode solution (1.8 or 2.0 mM) is significantly far from physiological Ca^{2+} concentrations in blood serum of humans (1.16–1.32 mM; Bell, 1995) and consequently, in the interstitial fluid, which represents the *in vivo* extracellular milieu. As far as the aim is a comparison of *in vitro* experimental data with the simulated electrical activity of cardiac cells, it is obviously correct to impose the same extracellular concentration used in experimental protocols. However using the same concentration can be incorrect when the analysis of *in vivo* pathophysiological mechanisms is the ultimate aim of simulation, as was the case for simulated hypocalcaemia and the compensatory effect of an increased sympathetic tone (Severi et al., 2009a).

Conclusion

This computational study explored interspecies differences between the extended Severi (rabbit) and Fabbri (human) SANC models to elucidate the

pathophysiological mechanisms of the elevated prevalence of SCD in HD patients. Furthermore we formulated and experimentally tested the hypothesis that increased sympathetic tone may compensate to some extent for hypocalcaemia-induced bradycardia, whereas sudden loss under hypocalcaemic conditions could lead to severe bradycardia and failure of the sinus node. By affecting the Ca^{2+} clock extracellular Ca^{2+} depletion was balanced by β-AR stimulation of critical membrane and SR currents. Whereas the Ca^{2+} cycling was directly affected by hypocalcaemia and the increased sympathetic tone, K^+ and Na^+ exchange played a subsidiary role, especially in the human-based SANC model. These findings could help to further understand the underlying pathomechanisms of SCD in CKD patients. Furthermore regular non-invasive point-of-care monitoring of electrolyte levels, especially $[Ca^{2+}]_o$, by ECGs could allow early diagnosis and continuous or retrospective assessment of plasma electrolyte concentrations (Pilia et al., 2020). This might be a possibility to reduce the high prevalence of SCD in CKD patients in the future.

References

American Heart Association. (2024). Target Heart Rates Chart. Advance online publication. https://www.heart.org/en/healthy-living/fitness/fitness-basics/target-heart-rates

Amsaleg, A., Sánchez, J., Mikut, R., & Loewe, A. (2022). Characterization of the pace-and-drive capacity of the human sinoatrial node: A 3D in silico study. *Biophysical Journal*, **121**(22), 4247–4259.

Barbuti, A., Terragni, B., Brioschi, C., & DiFrancesco, D. (2007). Localization of f-channels to caveolae mediates specific β2-adrenergic receptor modulation of rate in sino-atrial myocytes. *Journal of Molecular and Cellular Cardiology*, **42**(1), 71–78.

Behar, J., Ganesan, A., Zhang, J., & Yaniv, Y. (2016). The autonomic nervous system regulates the heart rate through cAMP-PKA dependent and independent coupled-clock pacemaker cell mechanisms. *Frontiers in Physiology*, **7**. https://doi.org/10.3389/fphys.2016.00419

Bell, C. A. (1995). Clinical guide to laboratory tests. 3rd edition. N. W. Tietz, ed. *Transfusion*, **35**, 972–972.

Bucchi, A. (2003). If-dependent modulation of pacemaker rate mediated by cAMP in the presence of ryanodine in rabbit sino-atrial node cells. *Journal of Molecular and Cellular Cardiology*, **35**(8), 905–913.

Bucchi, A., Baruscotti, M., Robinson, R. B., & DiFrancesco, D. (2007). Modulation of rate by autonomic agonists in SAN cells involves changes in diastolic depolarization and the pacemaker current. *Journal of Molecular and Cellular Cardiology*, **43**(1), 39–48.

Cuellar, A. A., Lloyd, C. M., Nielsen, P. F., Bullivant, D. P., Nickerson, D. P., & Hunter, P. J. (2003). An overview of CellML 1.1, a biological model description language. *Simulation*, **79**(12), 740–747.

Demir, S. S., Clark, J. W., & Giles, W. R. (1999). Parasympathetic modulation of sinoatrial node pacemaker activity in rabbit heart: A unifying model. *American Journal of Physiology-Heart and Circulatory Physiology*, **276**(6), H2221–H2244.

Di Lullo, L., Rivera, R., Barbera, V., Bellasi, A., Cozzolino, M., Russo, D., De Pascalis, A., Banerjee, D., Floccari, F., & Ronco, C. (2016). Sudden cardiac death and chronic kidney disease: From pathophysiology to treatment strategies. *International Journal of Cardiology*, **217**, 16–27.

Fabbri, A., Fantini, M., Wilders, R., & Severi, S. (2017). Computational analysis of the human sinus node action potential: Model development and effects of mutations. *The Journal of Physiology*, **595**(7), 2365–2396.

Harcourt-Brown, F. (2002). *Textbook of rabbit medicine*. Butterworth-Heinemann, Oxford.

Himeno, Y., Sarai, N., Matsuoka, S., & Noma, A. (2008). Ionic mechanisms underlying the positive chronotropy induced by β1-adrenergic stimulation in Guinea pig sinoatrial node cells: A simulation study. *The Journal of Physiological Sciences*, **58**(1), 53–65.

Itzhaki, I., Rapoport, S., Huber, I., Mizrahi, I., Zwi-Dantsis, L., Arbel, G., Schiller, J., & Gepstein, L. (2011). Calcium handling in Human induced pluripotent stem cell derived cardiomyocytes ed. Pera M. *PLoS ONE*, **6**(4), e18037.

Kohajda, Z., Loewe, A., Tóth, N., Varró, A., & Nagy, N. (2020). The cardiac pacemaker story—Fundamental role of the Na^+/Ca^{2+} exchanger in spontaneous automaticity. *Frontiers in Pharmacology*, **11**, 516.

Levy, M. N. (1971). Brief reviews: Sympathetic-parasympathetic interactions in the heart. *Circulation Research*, **29**(5), 437–445.

Loewe, A., Lutz, Y., Nagy, N., Fabbri, A., Schweda, C., Varro, A., & Severi, S. (2019). Inter-species differences in the response of sinus node cellular pacemaking to changes of extracellular calcium. In *2019 41st Annual International Conference of the IEEE Engineering in Medicine and Biology Society (EMBC)*, pp. 1875–1878. IEEE, Berlin, Germany. Advance online publication. https://ieeexplore.ieee.org/document/8857573/

Loewe, A., Lutz, Y., Nairn, D., Fabbri, A., Nagy, N., Toth, N., Ye, X., Fuertinger, D. H., Genovesi, S., Kotanko, P., Raimann, J. G., & Severi, S. (2019). Hypocalcemia-induced slowing of Human sinus node pacemaking. *Biophysical Journal*, **117**(12), 2244–2254.

Lyashkov, A. E., Juhaszova, M., Dobrzynski, H., Vinogradova, T. M., Maltsev, V. A., Juhasz, O., Spurgeon, H. A., Sollott, S. J., & Lakatta, E. G. (2007). Calcium cycling protein density and functional importance to automaticity of isolated sino-atrial nodal cells are independent of cell size. *Circulation Research*, **100**(12), 1723–1731.

MacDonald, E. A., Rose, R. A., & Quinn, T. A. (2020). Neurohumoral control of sinoatrial node activity and heart rate: Insight from experimental models and findings from humans. *Frontiers in Physiology*, **11**, 170.

Maltsev, V. A., & Lakatta, E. G. (2009). Synergism of coupled subsarcolemmal Ca^{2+} clocks and sarcolemmal voltage clocks confers robust and flexible pacemaker function in a novel pacemaker cell model. *American Journal of Physiology-Heart and Circulatory Physiology*, **296**(3), H594–H615.

Maltsev, V. A., & Lakatta, E. G. (2010). A novel quantitative explanation for the autonomic modulation of cardiac pacemaker cell automaticity via a dynamic system of sarcolemmal and intracellular proteins. *American Journal of Physiology-Heart and Circulatory Physiology*, **298**(6), H2010–H2023.

Pilia, N., Severi, S., Raimann, J. G., Genovesi, S., Dössel, O., Kotanko, P., Corsi, C., & Loewe, A. (2020). Quantification and classification of potassium and calcium disorders with the electrocardiogram: What do clinical studies, modeling, and reconstruction tell us? *Applied Physics Letters Bioengineering*, **4**(4), 041501.

Plank, G., Loewe, A., Neic, A., Augustin, C., Huang, Y.-L., Gsell, M. A. F., Karabelas, E., Nothstein, M., Prassl, A. J., Sánchez, J., Seemann, G., & Vigmond, E. J. (2021). The openCARP simulation environment for cardiac electrophysiology. *Computer Methods and Programs in Biomedicine*, **208**, 106223.

Poulikakos, D., Banerjee, D., & Malik, M. (2014). Risk of sudden cardiac death in chronic kidney disease. *Journal of Cardiovascular Electrophysiology*, **25**(2), 222–231.

Sacher, F., Jesel, L., Borni-Duval, C., De Precigout, V., Lavainne, F., Bourdenx, J.-P., Haddj-Elmrabet, A., Seigneuric, B., Keller, A., Ott, J., Savel, H., Delmas, Y., Bazin-kara, D., Klotz, N., Ploux, S., Buffler, S., Ritter, P., Rondeau, V., Bordachar, P., … Combe, C. (2018). Cardiac rhythm disturbances in hemodialysis patients. *The Journal of the American College of Cardiology: Clinical Electrophysiology*, **4**(3), 397–408.

Santini, M., Schneider, L., Bištirlić, M., Santini, J., Verunica, N., Lovrić-Benčić, M., & Zekanović, D. (2024). Case report: A unique case of sinus arrest and consequent symptomatic bradycardia caused by severe iatrogenic hypocalcemia. *Cardiologia Croatica*, **19**(11–12), 408–408.

Severi, S., Corsi, C., & Cerbai, E. (2009a). From *in vivo* plasma composition to *in vitro* cardiac electrophysiology and *in silico* virtual heart: The extracellular calcium enigma. *Philosophical Transactions of the Royal Society A*, **367**(1896), 2203–2223.

Severi, S., Corsi, C., Rocchetti, M., & Zaza, A. (2009b). Mechanisms of β-adrenergic modulation of IKs in the Guinea-pig ventricle: Insights from experimental and model-based analysis. *Biophysical Journal*, **96**(9), 3862–3872.

Severi, S., Fantini, M., Charawi, L. A., & DiFrancesco, D. (2012). An updated computational model of rabbit sino-atrial action potential to investigate the mechanisms of heart rate modulation. *The Journal of Physiology*, **590**(18), 4483–4499.

Stary, T., Linder, M., & Loewe, A. (2023). Sinoatrial node cell response to isoprenaline stimulation and hypocalcemia. *2023 Computing in Cardiology Conference*. Advance online publication. https://www.cinc.org/archives/2023/pdf/CinC2023-114.pdf

Trautwein, W., Cavalié, A., Flockerzi, V., Hofmann, F., & Pelzer, D. (1987). Modulation of calcium channel function by phosphorylation in guinea pig ventricular cells and phospholipid bilayer membranes. *Circulation Research*, 117–223.

Tsutsui, K., Monfredi, O. J., Sirenko-Tagirova, S. G., Maltseva, L. A., Bychkov, R., Kim, M. S., Ziman, B. D., Tarasov, K. V., Tarasova, Y. S., Zhang, J., Wang, M., Maltsev, A. V., Brennan, J. A., Efimov, I. R., Stern, M. D., Maltsev, V. A., & Lakatta, E. G. (2018). A coupled-clock system drives the automaticity of human sinoatrial nodal pacemaker cells. *Science signaling*, **11**(534), eaap7608.

Verkerk, A. O., & Wilders, R. (2023). Human sinoatrial node pacemaker activity: Role of the slow component of the delayed rectifier K^+ current, IKs. *The International Journal of Medical Students*, **24**(8), 7264.

Vinogradova, T. M., Bogdanov, K. Y., & Lakatta, E. G. (2002). β-adrenergic stimulation modulates ryanodine receptor Ca^{2+} release during diastolic depolarization to accelerate pacemaker activity in rabbit sinoatrial nodal cells. *Circulation Research*, **90**(1), 73–79.

Vinogradova, T. M., Sirenko, S., Lyashkov, A. E., Younes, A., Li, Y., Zhu, W., Yang, D., Ruknudin, A. M., Spurgeon, H., & Lakatta, E. G. (2008). Constitutive phosphodiesterase activity restricts spontaneous beating rate of cardiac pacemaker cells by suppressing local Ca^{2+} releases. *Circulation Research*, **102**(7), 761–769.

Virtanen, P., Gommers, R., Oliphant, T E., Haberland, M., Reddy, T., Cournapeau, D., Burovski, E., Peterson, P., Weckesser, W., Bright, J., Van Der Walt, S. J., Brett, M., Wilson, J., Millman, K. J, Mayorov, N., Nelson, A. R. J., Jones, E., Kern, R., Larson, E., … Vázquez-Baeza, Y. (2020). SciPy 1.0: Fundamental algorithms for scientific computing in Python. *Nature Methods*, **17**(3), 261–272.

Winter, J., & Shattock, M. J. (2016). Geometrical considerations in cardiac electrophysiology and arrhythmogenesis. *Europace*, **18**(3), 320–331.

Yang, D., Lyashkov, A. E., Li, Y., Ziman, B. D., & Lakatta, E. G. (2012). RGS2 overexpression or Gi inhibition rescues the impaired PKA signaling and slow AP firing of cultured adult rabbit pacemaker cells. *Journal of Molecular and Cellular Cardiology*, **53**(5), 687–694.

Yaniv, Y., Ganesan, A., Yang, D., Ziman, B. D., Lyashkov, A. E., Levchenko, A., Zhang, J., & Lakatta, E. G. (2015). Real-time relationship between PKA biochemical signal network dynamics and increased action potential firing rate in heart pacemaker cells. *Journal of Molecular and Cellular Cardiology*, **86**, 168–178.

Zaza, A., & Lombardi, F. (2001). Autonomic indexes based on the analysis of heart rate variability: A view from the sinus node. *Cardiovascular Research*, **50**(3), 434–442.

Zhao, Y., Chen, N. X., Shirazi, J. T., Shen, C., Lin, S.-F., Fishbein, M. C., Moe, S. M., & Chen, P.-S. (2016). Subcutaneous nerve activity and mechanisms of sudden death in a rat model of chronic kidney disease. *Heart Rhythm*, **13**(5), 1105–1112.

Additional information

Data availability statement

All data supporting the findings of this study are available within the paper or supplementary material.

Competing interests

The authors declare no competing interests.

Author contributions

M.L.: conception and design, analysis and interpretation of data, drafting, final approval of the manuscript, agreement to be accountable for all aspects of the work; T.S. analysis and interpretation of data, revising critically for important intellectual content, final approval of the manuscript, agreement to be accountable for all aspects of the work; G.B.: acquisition of data, drafting, final approval of the manuscript, agreement to be accountable for all aspects of the work; N.N.: acquisition of data, analysis and interpretation of data, revising critically for important intellectual content, final approval of the manuscript, agreement to be accountable for all aspects of the work; A.L.: conception and design, analysis and interpretation of data, revising it critically for important intellectual content, final approval of the manuscript, agreement to be accountable for all aspects of the work.

Funding

European High Performance Computing Joint Undertaking (EuroHPC): Moritz Linder, Tomas Stary and Axel Loewe, 955495; Deutsche Forschungsgemeinschaft (DFG): Moritz Linder, Tomas Stary and Axel Loewe, 507828355; NKFIH-OTKA: Norbert Nagy, 142949.

Acknowledgements

This work was supported by DFG-507828355 (CARPe-diem) and by the European High-Performance Computing Joint Undertaking EuroHPC under grant agreement number 955495 (MICROCARD) co-funded by the Horizon 2020 Programme of the European Union (EU); the French National Research Agency ANR; the German Federal Ministry of Education and Research; the Italian Ministry of Economic Development; the Swiss State Secretariat for Education, Research and Innovation; the Austrian Research Promotion Agency FFG; the Research Council of Norway; NKFIH-OTKA FK-142949; and the National Academy of Scientist Education.

Open access funding enabled and organized by Projekt DEAL.

Keywords

autonomic regulation, cAMP-protein kinase A (PKA) signalling, coupled clock mechanism, hypocalcaemia, sino-atrial node cells

Supporting information

Additional supporting information can be found online in the Supporting Information section at the end of the HTML view of the article. Supporting information files available:

Peer Review History
Supplementary Material